DEVELOPEMENT OF WIRELESS-POWERED IONIC POLYMER METAL COMPOSITES (IPMC) DEVICES FOR BIOMEDICAL APPLICATIONS

By

CHEONG HAU RAN

A dissertation submitted to the Department of Electrical and Electronics Engineering,
Lee Kong Chian Faculty of Engineering and Science,
Universiti Tunku Abdul Rahman,
in partial fulfillment of the requirements for the degree of
Master of Engineering Science
December 2018

ABSTRACT

DEVELOPMENT OF WIRELESS-POWERED IONIC POLYMER METAL COMPOSITES (IPMC) DEVICES FOR BIOMEDICAL APPLICATIONS

CHEONG HAU RAN

Ionic polymer-metal composite (IPMC) is an ionic electroactive polymer (EAP) that can be actuated at a low voltage, fast response and miniaturized, therefore, attracts significant interest that has led to extensive investigations, especially for biomedical applications. Conventional battery powered and wired interfaced IPMC actuator has limited mobility and poses the risk of battery leakage which is hazardous to human health. This project proposed an IPMC soft actuator that is controlled and powered in a wireless manner using magnetic resonant coupling as an effort to solve the mentioned constraint. The IPMC cantilever deflects when the external magnetic field (generated by the transmitter circuit) matches the resonant frequency of the LC receiver circuit (with IPMC actuator integrated). The proposed wirelessly powered IPMC actuator was demonstrated in biological cell manipulation application. A single active finger IPMC-based microgripper was fabricated by integrating the IPMC actuator to the developed planar resonant *LC* receiver and DC rectifier circuits. The fabricated prototype shows a maximum IPMC deflection of 0.765 mm (activation force of 0.17 mN) at the RF power of 0.65 W with 3.5 VDC supplied from the *LC* receiver circuit at the resonant frequency of ~13.6 MHz. Three repeated ON-OFF wireless activation cycle was performed

with the reported cumulative deflection of 0.57 mm. The cumulative deflection was increased to 1.17 mm, 1.19 mm and 1.24 mm for three different IPMC actuator samples respectively at 5 VDC supplied. As a proof of concept, fish egg was used to represent the biological cell manipulation operation. The microgripper successfully gripped the fish egg sample without creating any damages. Apart from the wirelessly powered microgripper, the wireless feature has been extended as an implantable drug delivery device. A 183 μm thick IPMC cantilever valve was attached with an embedded LC resonant circuit to wirelessly control the actuator when the field frequency is tuned to 25 MHz. Experimental characterization of the fabricated actuator showed a cumulative cantilever deflection of 160 μm for three repeated RF ON-OFF cycles at 0.6 W input power. The device was loaded with dye solution and immersed in DI water to demonstrate wireless drug release. Qualitative result shows the successful release of the dye solution from the device reservoir. The release rate can be controlled by tuning the RF input power. A maximum average release rate of ~0.1 μl/s was achieved. In-vitro study with human tumor cells (HeLa) has been further conducted to demonstrate the proof of concept of the developed device. Exclusively, the effectiveness of developed wirelessly powered IPMC actuator as biomedical devices has been validated with its effectiveness in soft microgripper and drug delivery application.

ACKNOWLEDGEMENT

I would like to thank my supervisor Dr. Chee Pei Song and my Co-supervisor Dr. Lai Koon Chun for guiding and assisting throughout my research projects. I am extremely grateful that they are willing to spend their time for having discussion with me. The valuable advice and ideas have contributed to the successful completion of my research.

Also, I would like to express my gratitude to UTAR for providing the research materials, equipments and facilities during my research. Moreover, the freely accessible online database has made research easier as all the valuable literatures are easily obtainable.

LEE KONG CHIAN FACULTY OF ENGINEERING AND SCIENCE

UNIVERSITI TUNKU ABDUL RAHMAN

Date: _____

SUBMISSION OF DISSERTATION

It is hereby certified that **CHEONG HAU RAN** (ID No: **17UEM00347**) has completed this dissertation entitled "DEVELOPMENT OF WIRELESS-POWERED IONIC POLYMER METAL COMPOSITES (IPMC) DEVICES FOR BIOMEDICAL APPLICATIONS" under the supervision of DR. CHEE PEI SONG (Supervisor) from the Department of Electrical and Electronic Engineering, Lee Kong Chian Faculty of Engineering and Science, and DR. LAI KOON CHUN (Co-Supervisor) from the Department of Electronic Engineering, Faculty of Engineering and Green Technology.

I understand that University will upload softcopy of my dissertation in pdf format into UTAR Institutional Repository, which may be made accessible to UTAR community and public.

Yours truly,

_____

(Cheong Hau Ran)

APPROVAL SHEET

This dissertation/thesis entitled "**DEVELOPMENT OF WIRELESS-POWERED IONIC POLYMER METAL COMPOSITES (IPMC) DEVICES FOR BIOMEDICAL APPLICATIONS"** was prepared by CHEONG HAU RAN and submitted as partial fulfillment of the requirements for the degree of Master of Engineering Science at Universiti Tunku Abdul Rahman.

Approved by:

_____

(Dr. CHEE PEI SONG) Date:……..
Supervisor
Department of Electrical and Electronics Engineering
Lee Kong Chian Faculty of Engineering and Science
Universiti Tunku Abdul Rahman

_____

(Dr. LAI KOON CHUN) Date:……..
Co-supervisor
Department of Electronic Engineering
Faculty of Engineering and Green Technology
Universiti Tunku Abdul Rahman

DECLARATION

I hereby declare that the dissertation is based on my original work except for quotations and citations which have been duly acknowledged. I also declare that it has not been previously or concurrently submitted for any other degree at UTAR or other institutions.

_____
(CHEONG HAU RAN)

Date _____

TABLE OF CONTENTS

LIST OF TABLES

LIST OF FIGURES

LIST OF SYMBOLS / ABBREVIATIONS

EAP	Electroactive polymer
IPMC	Ionic polymer metal composite
RF	Radio frequnecy
j	Current density
Q	Solvent transport flux
E	Electric field
∇p	Pressure gradient
AgNo	Silver nitrate
NaOH	Sodium hydroxide
SMP	Shape memory polymer
SMA	Shape memory alloy
MEMS	Microelectromechanical systems
WPT	Wireless power transfer
H	Magnetic field strength
x	Specific distance
I	Current circulating

r	Radius
n	Number of turns
M	Mutual inductance
k	Coupling coefficient
L	Self inductance
v	Induced voltage
μ_0	Magnetic costant
ω	Angular frequency
A	Area
f	Frequency
i	Current
C	Capacitor
d	Diameter
K	Layout dependent
ρ	Fill ratio
Cu	Copper
PI	Polyimide

Q	Quality factor
R	Resistance
P	Power
D	Transmission distance
PDMS	Polydimethylsiloxane

CHAPTER 1

INTRODUCTION

1.1 Background

Smart actuators, materials that change their physical dimensions corresponding to external stimulus, *i.e.* pH, temperature and electric potential, have gained significant attention in the biomedical community due to their abilities to control a multitude of active structures and devices. Various biomedical applications with the involvement of various smart actuators have been reported, including smart stent in detecting restenosis and occlusion (Chen et al., 2018), microgripper in cell manipulation (Cheong et al., 2018) and drug delivery devices for cancer treatment (Gensler et al., 2010). The actuation mechanism such as shape memory alloy (SMA) (Kim et al., 2006), shape memory polymer (SMP) (Zainal and Ali, 2016), piezoelectric (Ko et al., 2002), hydrogel (Ongaro et al., 2016), and electroactive polymers (EAPs) (Zamyad et al., 2018) have their physical properties change when subjected to external stimuli. Shape memory alloy (SMA), shape memory polymer (SMP) and hydrogel actuators change their shapes at temperature and pH differences whereas the EAP actuator deforms its size when stimulated by an electric field.

Electroactive polymers (EAPs) can be categorized as electric EAPs and ionic EAPs (Carpi et al., 2011). Electric EAPs produce large strain and

force when high electric field (>1 kV (Chee et al., 2016)) is applied, and this feature is favorable in high work density application such as industry robotics. Electrostrictive graft elastomer actuator (Bar-Cohen et al., 1999), dielectric elastomer actuator (DEA) (Hines et al., 2017) and ferroelectric polymer actuator (Mai et al., 2015) are actuators that are categorized as electric EAPs. Nonetheless, high operating voltage of the electric EAPs has limited its biomedical applications (Mirfakhrai et al., 2007). Ionic EAPs that operate at lower actuation voltage ~1-5 V are the promising candidate to overcome the mentioned issues (Ru et al., 2018). Ionic EAPs utilize ions movement to produce actuation. Hence, ionic EAPs are also known as 'wet' EAP as they require electrolyte phase for the ion movement. Conducting polymers, carbon nanotubes (CNTs) and ionic polymer metal composites (IPMC) are the actuators that fall in the ionic EAPs category (Mirfakhrai et al., 2007).

Among the ionic EAPs, IPMCs offer the advantages of low driving voltage, high deflection, light weight and ease of fabrication. IPMC consists of an anion exchange membrane (made of Nafion material) sandwiched between two thin layer of metal electrodes. When electric field is applied to the metal electrodes, the positive ions (cations) and water molecules migrate to the cathode, leaving the negative ions (anions) with the carbon chain. This molecule migration creates tensile stress in the cathode side whereas compression force is exerted in the anode side, causing the IPMC to bend.

1.2 Problem Statements

Despite the mentioned advantages of IPMC, it has not been fully exploited as biomedical devices. Earlier researches involve battery powered and wired interface circuitry to control the IPMC movement, which make the device bulky and highly invasive. Moreover, this approach limits the device mobility (Jiaqi et al., 2016, Ford et al., 2014). In the view point of biomedical device (*i.e.* drug delivery device), battery leakage is hazardous to human health. In addition, conventional IPMC packaging involves an external clamping electrode holder which has constrained the device size with limited longevity.

1.3 Research Objectives

1. To design and fabricate a wireless passive IPMC soft actuator that operates using RF magnetic field.
2. To characterize the developed IPMC soft actuator under wireless actuation.
3. To demonstrate the application of the developed actuator as biomedical device.

The main objective of this research is to develop a wireless powered IPMC actuator using a planar based LC receiver circuit controlled by the external radio-frequency (RF) magnetic field. The IPMC actuator is activated in a passive manner that eliminates the need for battery and active circuitry. The first task of this research is to design and fabricate a wireless passive

IPMC soft actuator that is operated using RF magnetic field. The developed wireless powered IPMC activated when the magnetic field of the integrated LC receiver circuit merged the field frequency of the transmitter circuit. After that, the fabricated prototype was characterized under wireless actuation. Finally, the wireless-powered IPMC actuator is applied as soft microgripper and drug delivery device as a proof of concept of biomedical applications.

1.4 Thesis Overview

In this dissertation, 6 chapters are reported. Chapter 1 introduces the background of the smart materials and the importance of the IPMC as ionic smart material is highlighted. The development of the IPMC actuator especially in biomedical applications is reviewed.

Chapter 2 reviews the working principle of the IPMC and the performances of the IPMC are compared with other reported EAPs actuators. The wireless power transfer systems and the design parameters are studied.

In Chapter 3, the planar-based LC receiver circuit is designed, fabricated and characterised. The characterisation such as resonant frequency behaviour at different operating media, transmission efficiency at different distances and tilting angles are examined.

In Chapter 4, a wireless-powered IPMC-based soft microgripper is reported to show the wireless powered IPMC fabricated prototype in

biomedical applications. The description of the design, working principle and fabrication procedure will be presented in detail. The analysis of the device will be discussed with simulated and measured results.

In Chapter 5, the wireless-controlled drug delivery device is presented using IPMC-based cantilever valve. This is to show the fabricated prototype's application in drug delivery device. The design and working principles are presented in the following sub section. It is then followed by the fabrication procedure of the device and the analysis of the device.

In Chapter 6, the research works are summarised with the proposal of future works to improve the device's performances.

CHAPTER 2

LITERATURE REVIEW

2.1 Introduction of IPMC

IPMC is an ionic polymer in a composite form, sandwiched between electrodes. It exhibits large dynamic deformation at an applied electric field. IPMC shows a great potential as soft robotics actuator, artificial muscles and dynamic sensors. The fundamental of the IPMC with regard to its working principle, fabrication process, characterization and application are further explained in the subsequent subsections.

2.1.1 Working Principle of IPMC

IPMC is made of ion exchange polymers such as Flemion (perfluorocarboxylate, produce by Asahi Glass, Japan) (Arumugam, 2012) or Nafion (perfluorosulfonate produced by DuPont) that allows ion transportation at an applied electric field. To induce electric potential, the polymer surface is deposited with a conductive layer such as platinum or gold to act as electrode. The hydrated mobile cations in the ion exchange membrane attracts to the cathode through anionic tunnel, which is formed by the polymer side chains, at an applied electric potential. As presented in Figure 2.1, the cation migration drags water molecules along and swells the ion exchange membrane. The

deflection of the membrane depends on the applied potential where large deflection is anticipated at high voltage. The direction of the deflection can be altered by controlling the polarity of the potential difference. (Shen et al., 2013, Wang et al., 2013).

Based on the mentioned working principle, IPMC can also work as a sensor. At an applied force, mobile cations in the membrane move from the original location to another location and they generate a potential difference between two electrodes. This potential difference can be amplified for readable signal. Figure 2.2 illustrates the fundamental principle of IPMC for sensing motion. The cation migration depends on the frequency of an applied displacement, as mentioned in (Nelson, 2015).

The working principle of the IPMC can be modelled to predict the transducer performance. Gennes et. al. (De Gennes et al., 2000) reported a standard Onsager formulation which uses linear irreversible thermodynamics equation. Under static conditions, the deflection performance of the IPMC is modelled based on mechanoelectric effect: ion transport (current density, *J*, normal to the material) and solvent transport (flux, *Q*, this term is referred as water flux). The conjugate forces involve the electric field, *E*, and the pressure gradient, $-\nabla \mathrm{p}$ can be expressed as:

$$J = \sigma E - L_{12} \nabla \mathrm{p} \tag{2.1}$$

$$Q = L_{21} E - \mathrm{K} \nabla \mathrm{p} \tag{2.2}$$

where σ and K are the membrane conductance and the Darcy permeability, respectively. The cross-coefficient is denoted as $L_{12} = L_{21} = L$, experimentally measured as 10^{-8} (ms^{-1}/ Vm^{-1}).

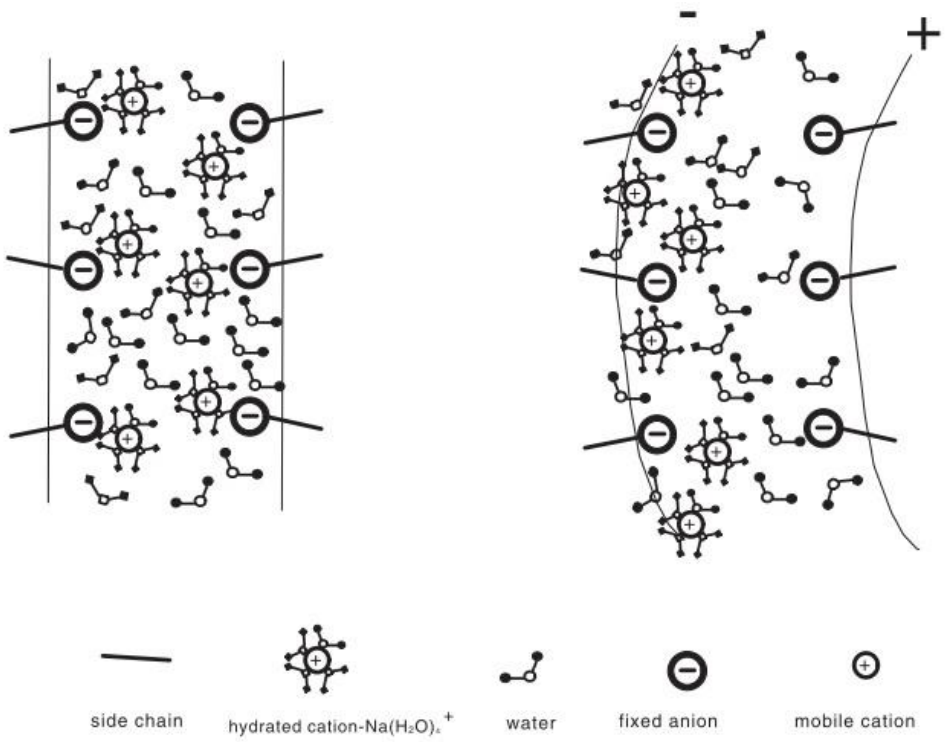

Figure 2.1: Schematic diagram of the IPMC artificial muscle and its ion exchange principle (Shahinpoor and Kim, 2001)

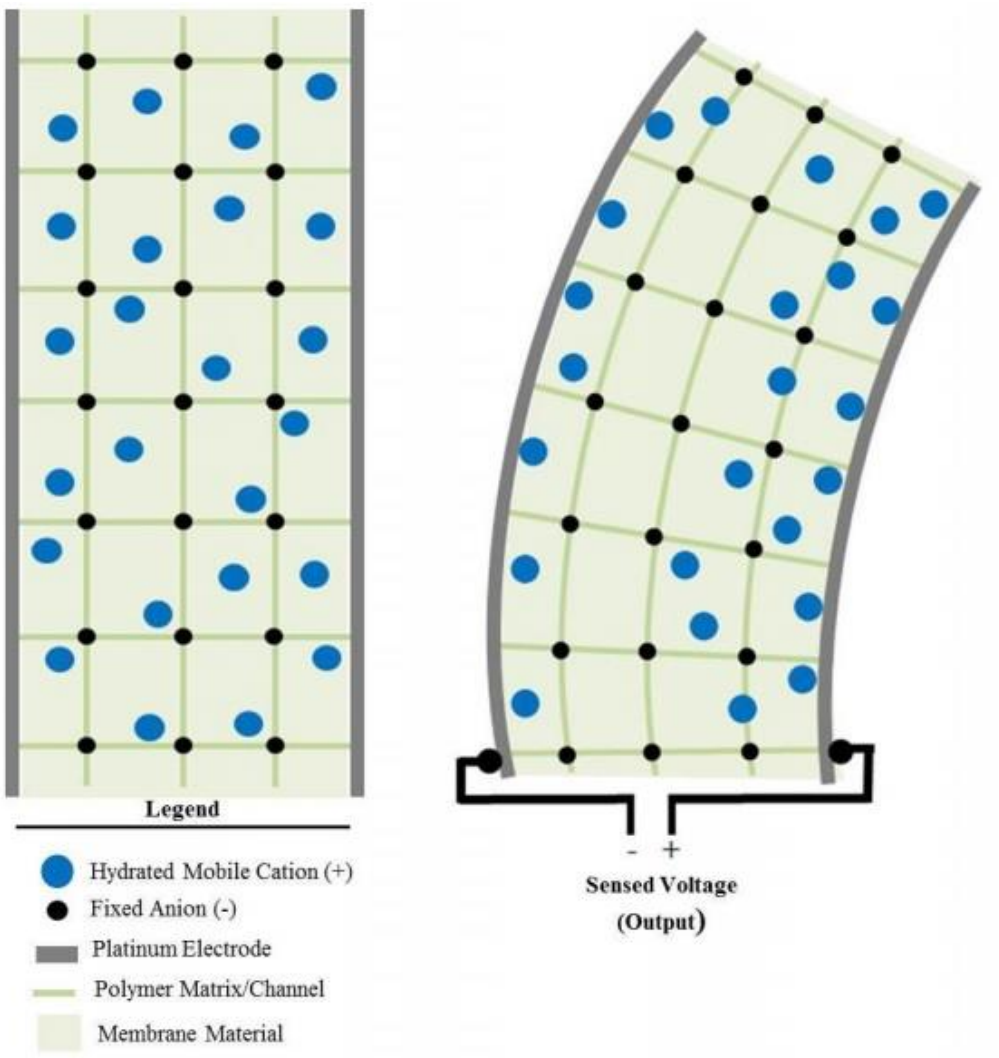

Figure 2.2: Migration of cations in IPMC sensing mode (Nelson, 2015)

2.1.2 Fabrication of IPMC

IPMC transducer is constructed by depositing noble metals such as platinum, gold or silver to ion exchange membrane surface. In the following subsections, the commercially available ion exchange membrane and the metal depositing process are explained.

2.1.2.1 Ion Exchange Membrane

Ion exchange membrane is the basic materials of IPMC which permit the ions transportation when the membrane is hydrated, which has been mentioned in the preceding section. Nafion® and Flemion® are the conventional ion exchange membranes that are utilized in IPMC. As compared with Flemion, Nafion material is more favourable due to its ease of availability. DuPont™ is the primary supplier for Nafion® products. Various thicknesses of prefabricated Nafion® ion exchange membranes are offered by DuPont™. Generally, These membranes are utilized in the fuel cell industry (Nelson, 2015).

Prefabricated Nafion® membranes are limited to the fixed thickness. *Ion Power Inc* offers extrusion-cast non-reinforced and reinforced dispersion-cast Nafion® sheets ranging in thicknesses from 0.025 mm to 0.254 mm. A summary of the available membrane thicknesses from DuPont™ Nafion® that can be purchased from *Ion Power Inc* are shown in Table 2.1 (Nelson, 2015). Dispersion-cast Nafion® membrane is manufactured through liquid polymer dispersion; while the extruded Nafion® is extruded from die. In this project, the DuPont™ Nafion® sheet with the model number N 117 was chosen as the IPMC's membrane as its thickness is well suited for the biomedical applications.

Table 2.1: Nafion® sheets that are available commercially from Ion Power, Inc (Nelson, 2015)

DuPont™ Nafion® Sheet (Ion Power, Inc)		
Model Number	Dry Thickness (mm)	Manufacturing Process
NR-211	0.025	Dispersion-Cast
NR-212	0.051	Dispersion-Cast
N 115	0.127	Extrusion
N 117	0.183	Extrusion
N 1110	0.254	Extrusion

2.1.2.2 Deposition of Metal Electrodes on the Surface of IPMC

Carbon composite electrode and metal electrode are the conventional electrodes that are used by IPMC actuator. Carbon composite electrode consists of graphite, graphene oxide, single wall carbon nanotube and multi-wall carbon nanotube (Lee and Yoo, 2011). On the other hand, platinum, gold, copper and silver are the few examples which are most commonly used as the metal electrode (Shahinpoor, 2015). However, the selections of materials for the electrode are depending on the conductivity and the suitability of the membrane applications. For instance, platinum is a commonly used electrode for biomedical application as it is magnetic resonance imaging (MRI) compatible. It does not affects the magnetic field from the MRI machine and computed tomography (CT) scans (Shahinpoor, 2015). However, the availability of the platinum and gold in the market is low and their costs are higher among the commonly used metal electrodes.

Silver material with the advantages of high availability and low cost is more favourable as deposited material. To deposit the electrode, electroless plating process is utilized (Lei and Tan, 2013, Shaari et al., 2014, Zhang et al., 2007). The plating process involves primary plating (reduction), secondary plating and ionic absorption. The details of the fabrication recipe have been mentioned in (Ong, 2016).

Firstly, the design of the IPMC was firstly cut into a desired dimension prior to blasting process. The blasting process is to increase the surface area density (Zhang et al., 2007) of the electrodes to ease the adhesion of the metal layer. The Nafion 117 was thoroughly cleaned in the mixture of sulfuric acid (H_2SO_4) and hydrogen peroxide (H_2O_2).Then, the silver layer was plated on both of the Nafion-117 surfaces (top and bottom) using silver mirror electroless plating process (Chen et al., 2009) by dipping the Nafion-117 in a complex solution of $[Ag(NH_3)_2]OH$, mixture of 1.6 g sodium hydroxide, 1.2 g silver nitrate, 2 g ammonia solution (28%) and 120 g DI water for 5 minutes The Nafion-117 later was transferred to another solution (mixture of 0.8 g glucose, 120 g DI water) for 5 minutes. The silver electrodes were formed with the following chemical reactions:

$$2\ AgNO_3 + 2\ NaOH \rightarrow Ag_2O + 2\ NaNO_3 + H_2O$$

$$Ag_2O + 4\ NH_3 + H_2O \rightarrow 2\ [Ag(NH_3)_2]OH + 2\ H_2O$$

$$CH_2OH(CHOH)_4CHO + 2\ [Ag(NH_3)_2]OH \rightarrow 2\ Ag + CH_2OH(CHOH)_4COONH_4 + 3\ NH_3 + 3\ H_2O.$$

The plated membrane was later submerged in a 1M solution of lithium chloride for 24 hours to initiate replacement of the hydrogen ions with lithium ions. According to (Stalbaum et al., 2014), the utilisation of lithium ion as the cation produces better electromechanical performance.

Numerous improved electroplating methods with low cost and times saving features are introduced. Physical loaded and interlock (PLI) replaces the conventional electroless plating process by using hot-press machine. The fabrication details have vividly been mentioned in (Ong, 2016). Besides the PLI method, others such as vacuum evaporator, sputtering coater and e-beam deposition with the advantages good surface finishing have been utilized in forming the electrode on the Nafion surface.

2.1.3 Characterization of IPMC as actuator

Shaari et al. (Shaari et al., 2014) reported the IPMC tip force and displacement characterization at different thicknesses (190 μm, 360 μm and 450 μm) at lengths (30 mm, 40 mm and 50 mm). As shown in Figure 2.3, the result shows that the tip forces of the IPMC increase linearly, proportional to the driven voltage with larger force produced at thicker structure. In other word, the tip force of the IPMC can be enhanced by increasing the thickness of the membrane. The displacement of the IPMC, on the other hand, depends on the device length. Figure 2.4 shows that the displacement of IPMC increases with the membrane length at lower input frequency range of the

driving voltage. High frequency limits the accumulation time of the mobile cation at the cathode and it reduces the displacement.

In addition, trade-off behaviour was observed in the IPMC where longer IPMC has low force produce. (Lee et al., 2006) Figure 2.5 shows different lengths of IPMCs with 200μm thick with their tip forces measured from 1.5 V to 4 V. The result shows that shorter IPMC actuator generates a larger actuating force; however, the displacement reduces as a trade-off to the actuating force. Figure 2.5 shows non-linear behaviour of the supplied voltage when it increases to 3.5 V. The sudden drop of the tip force might be caused by the voltage overdrive that lead to electrolysis phenomena, as mentioned in (Lee et al., 2006).

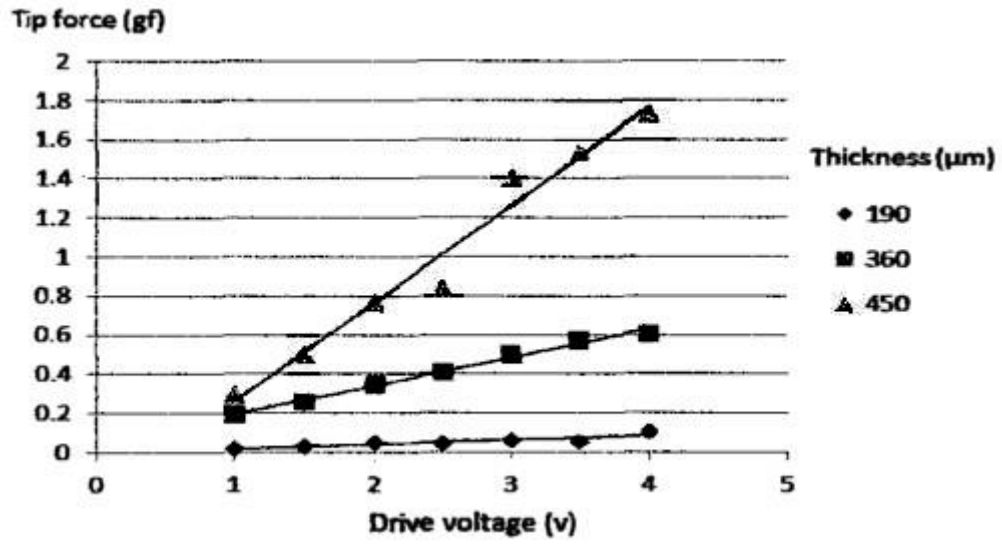

Figure 2.3: Tip force generated by IPMC artificial muscle at different actuation voltage levels (Shaari et al., 2014)

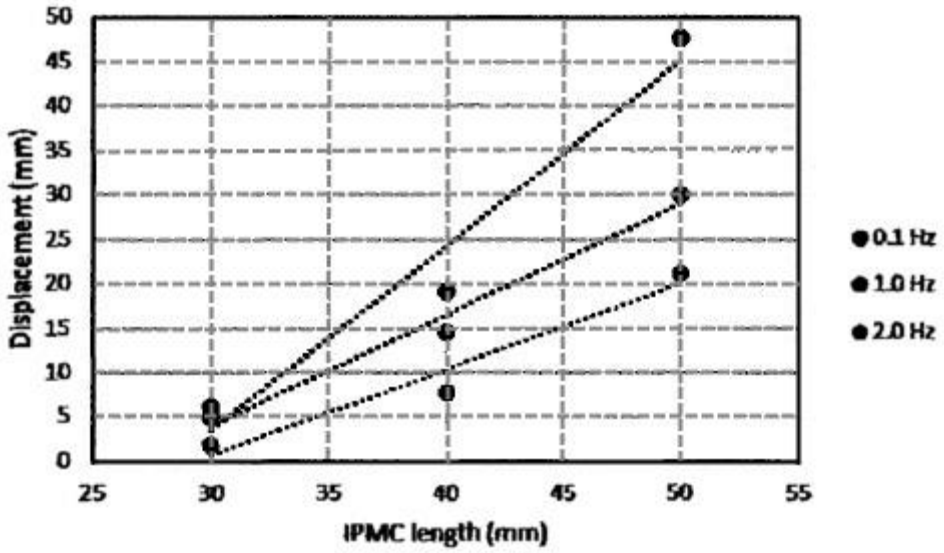

Figure 2.4: IPMC displacement against IPMC length

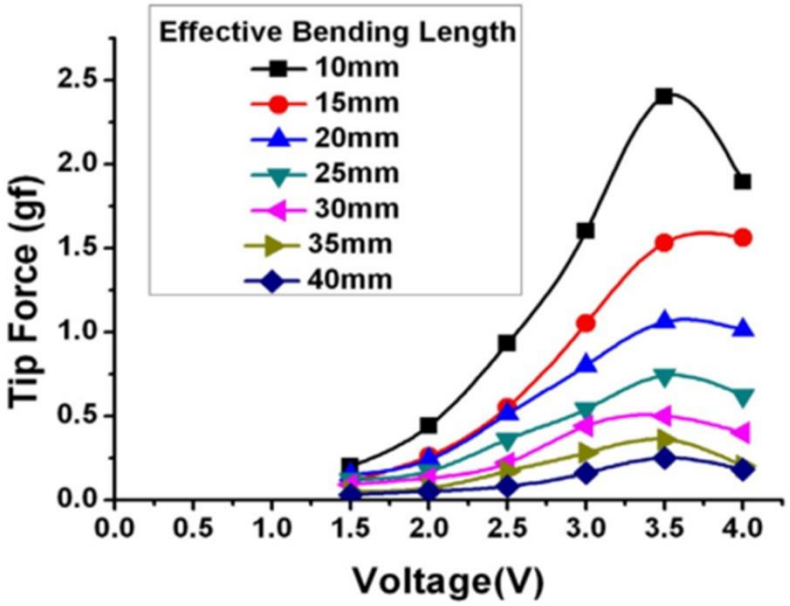

Figure 2.5: Tip force of IPMC with respectively effective bending length (Lee et al., 2006)

2.1.4 Applications of IPMC in Dry and Wet Environments

IPMC demonstrates the electroactive behaviour in both dry and wet environments (Shahinpoor and Kim, 2004). Due to this advantage, IPMC has

been widely used for industrial operations such as assembly of microsystem for microelectromechanical system (MEMS) (Lumia and Shahinpoor, 2008). In this section, the development efforts in utilizing the IPMC as the actuator in both dry and wet environment are explored.

Bhattacharya et al. (Bhattacharya et al., 2017) reported an IPMC based glove working in dry environment for object identification purposes. In this report, the IPMC functioned as a sensor which can generate different voltage patterns using an oscilloscope based on different types and shapes. In addition, IPMC was used to mimic legs and applied to a walking robot (Nguyen et al., 2015). The walking motion was controlled by the IPMC actuator which was manipulated by a programmed controller. Despite the dry environment application, Chen et al. (Chen et al., 2010) presented a battery powered robotic fish and IPMC-based manta ray robotic fish.

2.1.5 Comparison of IPMC with Other Smart Materials.

MEMS actuator can be categorized into several actuation mechanisms including electrostatic (Mukundan and Pruitt, 2009), thermal (Suma et al., 2012) and electric actuations (Palmre et al., 2013). Table 2.2 summarizes the performances of different smart materials at different actuation mechanisms based on their deflections (mm) per unit dimension (mm^3) ratios.

In MEMS, electrostatic actuations mechanism has minimal energy loss and simple structure (Fujita, 1989). However, their deflections are usually low

and they require voltage as high as 0.004375 mm^{-2}. Spark formation in the electrostatic actuation might cause dangerous issues (Goldsmith et al., 2001).

Thermal actuation materials such as shape memory polymer (SMP) and shape memory alloy (SMA) have better deflection per unit dimension than electrostatic actuation. However, thermal actuation tends to have high power consumption and sensitive to environment (Ali and Sultan, 2012). Changes of temperature in the operating environment might cause failing of actuator activation or over-performing. Such issues might limit the devices practicability.

The piezoelectric membrane is well known for its high force potential fast dynamic response time and repeatability (Huber et al., 1997). Despite the advantages, it requires high driving voltage and its actuation range is small with the deflection per unit dimension of 0.22 mm^{-2} at 30 V activation voltage. High operating voltage was also applied to dielectric elastomer, as shown in Table 2.2. The performance of this material can be as low as 0.00045 mm^{-2} with the driving voltage of 4.2 kV. The low actuations of the piezoelectric and dielectric elastomer are undesirable for biomedical application.

IPMC offers simplicity in fabrication method, fast bending movement and large displacement with low driving voltage (Bhandari et al., 2012). As shown in Table 2.2, the reported IPMC has the best performance among the MEMS actuators with its high deflection at low operating voltage.

Table 2.2: Review on smart materials and its actuation mechanism

Smart Materials	Stimuli	Deflection/Dimension [mm^{-2}]	Voltage [V]
Silicon membrane (Benmoussa et al., 2014)	Electrostatic	0.004375	10
SMP (Zainal and Ali, 2016)	Thermal	0.021	n/r
SMA (Xu et al., 2001)	Thermal	0.0278	n/r
Piezoelectric membrane (Ko et al., 2002)	Electric	0.22	30
Dielectric elastomer (Ghazali et al., 2017)	Electric	0.00045	4200
IPMC (Cheong et al., 2018)	Electric	0.22	5

2.2 Wireless Power Transfer: Background, Theory and Analysis

In recent years, wireless power transfer (WPT) has gained significant interest due to its broad applications in electrical vehicles (AFRIDI, 2018), consumer electronics (Chatterjee et al., 2003, Baker et al., 2007) and implantable medical devices (Li et al., 2015, Si et al., 2008). Numerous WPT schemes have been reported, including coupled electric fields, electromagnetic induction (Brown, 1984), radio frequency (RF) and microwave (Boys et al., 2000), inductive coupling (Valtchev et al., 2012), and magnetic resonant coupling (Hoang and Bien, 2012). Taking the consideration of device size, safety, distance and efficiency, utilizing magnetic resonant coupling as the powering scheme could be very beneficial, as discussed in (Moghadam and Zhang, 2016). Magnetic resonant coupling uses a pair of coupled coils and capacitance to tune the resonant frequency of the receiver to merge the field frequency of the transmitter. This technique provides high power transmission efficiency with longer transmission distance than the conventional inductive coupling scheme (Kim et al., 2013).

Based on the mentioned advantages, magnetic resonant frequency scheme has been chosen as the wireless powering scheme in this project. In the subsequent section, the fundamental of the WPT such as working principle, design and fabrication, and coupling coefficient are analysed and reviewed.

2.2.1 Working Principle of WPT via Magnetic Resonant Coupling

Magnetic resonant coupling wireless power transfer scheme uses similar concept with the transformer where power is wirelessly transferred using a pair of transmitter and receiver coils. The transmitter coil acts as the energy source and the receiver coil functions as the energy collector. The transmission of energy is in the form of magnetic field, which is generated by the transmitter. Figure 2.6 illustrates the working principle of the WPT between the transmitter coil and receiver coil via magnetic coupling. The alignment of the transmitter and receiver is important to ensure maximum power transfer. The circuit can be used to illustrate WPT via magnetic resonant coupling is depicted in Figure 2.7 presented by (Vinge, 2015). The voltage v_g is supplied by the function generator with resistance r_g. The energy is transferred between the two circuits based on inductive coupling of the two coils over an air gap, with self-inductance L_1, and L_2 and mutual inductance M. The two capacitors C_1 and C_2 can be adjusted to control the performance of the WPT system and R_L represent the load. Based on *Kirchhoff's voltage and current law* the circuit can be expressed as following equations (Vinge, 2015):

$$v_g - r_g i_1 - \frac{i_1}{j\omega C_1} - v_1 = 0 \tag{2.3}$$

$$i_2 + j\omega C_2 v_2 + \frac{v_2}{R_L} = 0 \tag{2.4}$$

where v_1 and v_2 are related to i_1 and i_2 by Faraday's Law:

$$v_1 = j\omega L_1 i_1 + j\omega M i_2 \tag{2.5}$$

$$v_2 = j\omega M i_1 + j\omega L_2 i_2 \tag{2.6}$$

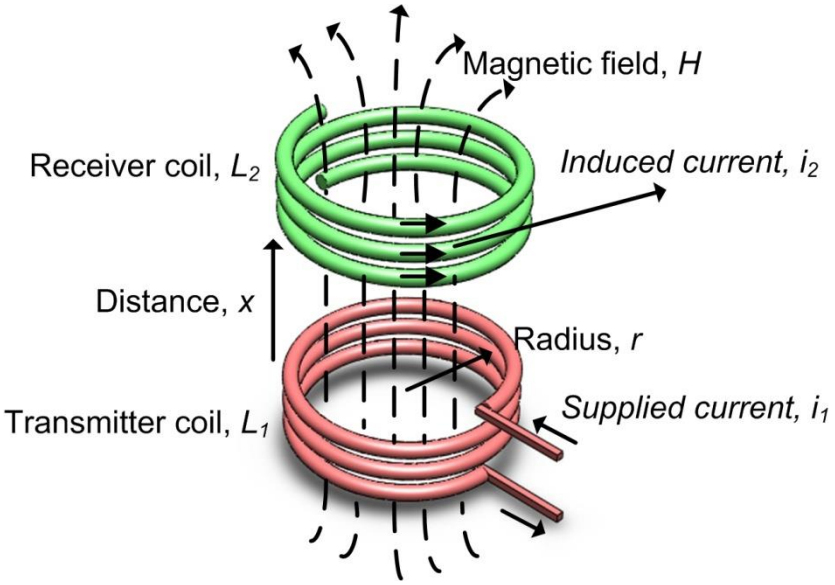

Figure 2.6: Working principle of WPT between transmitter coil and receiver coil

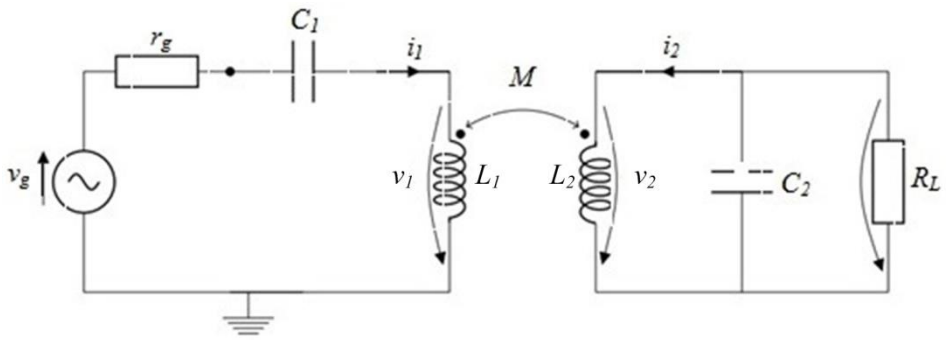

Figure 2.7: Circuit diagram modeling the WPT via magnetic resonant coupling system (Vinge, 2015)

The magnetic field generated at the transmitter coil when alternating current flows through the coil According to Ampere's Law, the magnetic field strength, *H*, can be expressed as a function of a specific distance, *x* as the following equation (Deyle and Reynolds, 2008):

$$H(x) = \frac{I \times n_t \times r^2}{2\sqrt{(r^2 + x^2)^3}} \tag{2.7}$$

where I, r and n_t, are the current circulating, radius and number of the turns of the transmitter coil, respectively. The magnetic coupled of the transmitter and the receiver forms a mutual inductance, M, which can be expressed as the following equation (Flack et al., 1971):

$$M = k\sqrt{L_1 L_2} \tag{2.8}$$

where k is denoted as the coupling coefficient, L_1 and L_2 are the self inductance of transmitter coil and receiver coil, respectively. Alternating current is induced at the receiver when its resonant frequency merges the transmitter's magnetic field. The induced alternating current can be converted into induced voltage, v, which can be expressed using Faraday's Law (Deyle and Reynolds, 2008);

$$v = \mu_0 H \omega n_p A_p \tag{2.9}$$

where μ_0 is the magnetic constant, ω is the angular frequency. n_p and A_p are the number of turns and the area of the receiver coil, respectively.

2.2.2 Design and Fabrication of Planar-based Resonant Circuit

Planar-based WPT has been widely used in MEMs applications especially for biomedical devices (Sarraf et al., 2009, Ali and Takahata, 2010). This is mainly due to the small space occupied and the simplicity of the fabrication method. There have been some efforts on modeling and design of planar-based resonant circuit (Merrill et al., 1995, Yue et al., 1996).

To design the planar-based WPT, the resonant frequency, f_r can be designed by connecting the inductor, L and capacitor, C in parallel to form the LC resonant circuit based on the given equation:

$$f_r = \frac{1}{2\pi\sqrt{LC}} \tag{2.10}$$

The coil inductance in spiral shape can be determined from the equation of *Modified Wheeler Formula,* (Mohan et al., 1999):

$$L_{mw} = K_1 \mu_0 \frac{n^2 d_{avg}}{1 + K_2 \rho} \tag{2.11}$$

where ρ represents the fill ratio which is expressed as $\rho = (d_{out} - d_{in}) / (d_{out} + d_{in})$. K_1 and K_2 are the layout dependent and n is the number of turns of the coil. d_{avg} is the average diameter of the coil, which is calculated from $d_{avg} = 0.5 (d_{out} + d_{in})$, where d_{out} and d_{in} are the outer diameter and the inner diameter

of the planar spiral coil. The design parameters for different inductor shapes are presented in Figure 2.8.

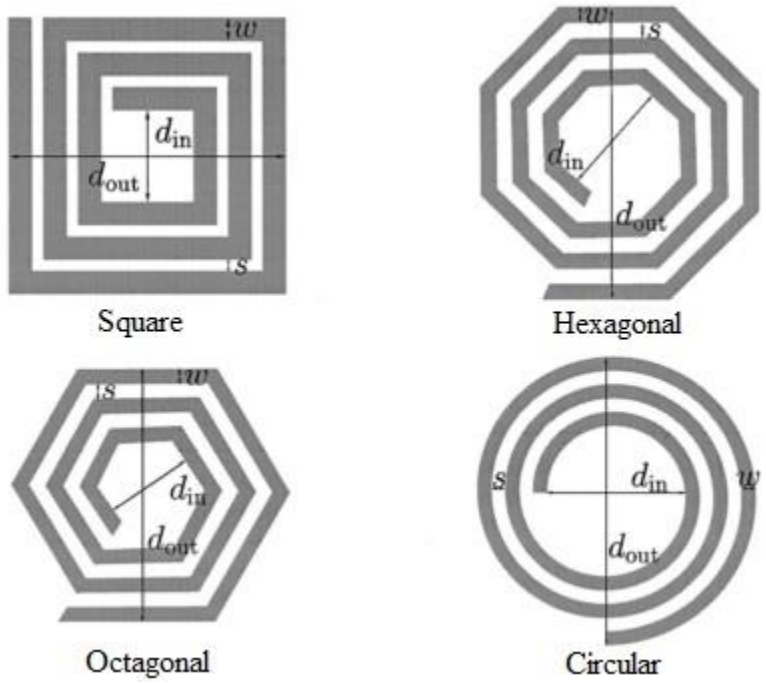

Figure 2.8: Planar spiral inductor geometry involved square, hexagonal, octagonal and circular (Mohan et al., 1999)

The value of capacitance, *C* can be expressed from the following equation:

$$C = \frac{\varepsilon_0 \varepsilon_r A}{d} \tag{2.12}$$

where ε_0 is the air permittivity, ε_r is the dielectric constant of the materials between the capacitor parallel plate.

To fit the device for biomedical applications, material selectivity plays an important role to ensure no side effects from the fabricated device to the human body. Copper-clad polyimide (PI) has been widely implemented in

implantable devices due to its soft and biocompatibility properties (Sridhar, 2008). Furthermore, PI can be fabricated using the printed-circuit-board technology which is simple compared to photolithography process.

2.2.3 Key Performance Parameter for Magnetic Resonant coupling

The performances of the WPT can be analysed based on the receiver's resonant frequency, coil resistance, quality factor, coupling coefficient, and transmission distance.

2.2.3.1 Resonant Frequency

Resonant frequency is the frequency when the transmitter and receiver have minimum impedance and hence produces larger response, compared to other frequency range. The resonant frequency value is designed based on the inductance, L and capacitance, C value of the resonant circuit, which can be expressed from the equation (2.10).

By fixing the outer diameter of the transmitter or receiver coil and the number of turns of the coil, the line width is inversely proportional to the inner diameter of the coil, which means that when the line width increases, the inner coil diameter will decrease. Since the inner turns are closer to the centre of the spiral coil, it makes the coils to have smaller L and thus contributes lesser mutual inductance (Mohan et al., 1999). This phenomenon would affect increment of the resonant frequency of the resonant circuit.

From the *Modified wheeler formula* (2.11) mentioned in previous section, number of turns, n is linearly proportional with the inductance value, L of the coil. Therefore, by increase n, the value of L will increase and cause an exponentially decrease of resonant frequency, f_r and vice versa.

2.2.3.2 Quality Factor

Coil resistance is also one of the important parameters in WPT via magnetic resonant coupling. The power transmission efficiency relies on the quality factor of the transmitter and receiver circuit. Quality factor, Q is defined as the ratio of energy stored to the energy dissipated in the resonator coil. It is defined as following equation:

$$Q = \frac{\sqrt{L}}{R\sqrt{C}} \tag{2.13}$$

The coil resistance, R is expressed as:

$$R = \frac{\rho l}{A} \tag{2.14}$$

where ρ is denoted as the coil material resistivity, l is the length of the coil and A is the cross sectional area of the coil.

From the equation, it is worth noting that the coil resistance increases when the coil surface area, A decreases, which degrades the Q value. In

addition, the presence of Eddy current that is induced to flow in the opposite direction of the supplied current is an undesirable element in magnetic resonant coupling system. This phenomenon is also named as skin effect, which leads to the increase of coil resistance, *R* and degrades the Q value. When the resonant circuit operates at high frequency, which is called as skin effect that will shift the eddy current to the surface of the coil, and results in an uneven current distribute at the coil line leads to an increase of the effective resistance at of the coil (Ali and Sultan, 2012).

On the other hand, by varying the *n* of the coil could have changed of the total length of the coil, and thus affecting the *R*. From equation (2.14), length of the coil, *l* is linearly proportional with the resistance value, *R* of the coil. Therefore, by increase *n*, the value of *l* will increase and it causes an exponentially degrade of quality factor, *Q* and vice versa.

2.2.3.3 Coupling Coefficient

Coupling coefficient, *k* describes the coupling strength of the two coils. It can be expressed from the mutual inductance equation as:

$$k = \frac{M}{\sqrt{L_1 L_2}} \tag{2.15}$$

where L_1 and L_2 are the self-inductance of the coils that depends on the line width and number of coils. *k* is denoted within the range of 0 to 1 to represent the coupling state. Increasing and decreasing of the number of turns and line

width can affect the overall efficiency of the WPT. From the equation (2.5) and (2.6) mentioned in previous section, mutual inductance, *M* is linearly proportional with the induced voltage, *v* in the secondary coil of the coil. Therefore, by increasing *n* or decreasing *l* of coil, the value of *L* will increase and it causes an increase of mutual inductance, *M* and vice versa. Since *M* is linearly proportional to, *v*, hence, increase in *M* will lead to an increase of induces voltage, *v*.

The coupling between the transmitter and receiver coils is relied on the mutual inductance, *M*, which can be expressed as based on (Patrick and Fardo, 2008):

$$2M = L_{total} - L_T - L_R \tag{2.16}$$

where L_{total} is the total measured inductance value when both transmitter inductance coil, L_T and receiver inductance coil, L_R are connected in series and aligned. When the transmitter and receiver coils are aligned in-phase, the total inductance is larger than the sum of their individual inductances. The difference between the measured L_{total} and the sum of individual L_S is twice of the mutual inductance.

2.2.3.4 Wireless Power Transfer

Based on (Sarraf et al., 2009), the power consumed in the receiver coil can be calculated from the following equation:

$$P(\omega) = \frac{R_0 v^2}{[R_0 + j\left(\omega L - \frac{1}{\omega C}\right)]^2} \tag{2.17}$$

where v is the voltage induced in the receiver coil and R_o is the parasitic resistance of the circuit. When the magnetic field frequency produced from transmitter circuit matches with the resonant frequency of the receiver circuit, the reactance will be eliminated, and hence, it maximizes the power transfer. The equation can be rewritten as:

$$P(\omega_r) = \frac{v^2}{R_0} \tag{2.18}$$

where ω_r is the angular frequency at resonant frequency of the receiver circuit.

The power transfer of the transmitter circuit and the receiver circuit through mutual inductance coupling is depicted as, P_T. The power induced at the receiver circuit is expressed as:

$$P_R = P_T \frac{M}{L_T} \tag{2.19}$$

By substituting the mutual inductance equation (2.8) into (2.19), P_R can be rewritten as:

$$P_R = P_T \frac{k\sqrt{L_T L_R}}{L_T} \tag{2.18}$$

and the power transfer efficiency, η, can be calculated as:

$$\eta = \frac{P_R}{P_T} = k\frac{L_R}{L_T} \tag{2.19}$$

From equation (2.10) and (2.11), it is worth noting that the coil inductance is reduced with the increase of the width of the coil and hence, leading to the decrease of power transfer efficiency. Under a fixed width line (due to the fabrication constraint), the inductance of the coils can be enhanced by increasing the number of turns.

2.2.3.5 Distance Characterization

In magnetic resonant coupling wireless power transmission, the power transfer decreases with the separation distance between transmitter and receiver due to the reduction of *k*. Therefore by varying the value of line width and number of turns, the *k* value which could affect the distance transfer and influence the power efficiency of the WPT. Since coupling coefficient, *k*, is linearly proportional to the mutual inductance, *M* of the coils as expressed in equation (2.15), hence increase of number of turns, *n* and decrease of line width of the coils leading to an increase of coupling coefficient, *k* and vice

versa. From equation (2.19), k has a linearly proportional relation with power efficiency, η, thus k increase will lead to an exponential increase of power efficiency and vice versa.

2.3 IPMC-based Biomedical Applications

IPMC offers advantages of flexible and biocompatible, making it as a promising candidate for numerous applications, especially in biomedical applications, which involve human organs or tissue contact (Zhang et al., 2012), such as artificial ventricular muscles, surgical tools and drug delivery devices. In this section, possible applications of IPMC materials for biomedical engineering are explored.

2.3.1 Drug Delivery Devices

Jiaqi et al. (Jiaqi et al., 2016) reported an IPMC-based valveless pump for drug delivery applications. The IPMC actuation is controlled by a controller with LabVIEW program. Figure 2.9 illustrates the geometrical structure of the valveless pump. The IPMC deflects the pump's diaphragm and induces the flow into the chamber. This design features bi-directional flow properties and good pumping performance was demonstrated through experiments. However, the controller tends to make the device size larger, and the wired interface of the system could limit the mobility of the pump.

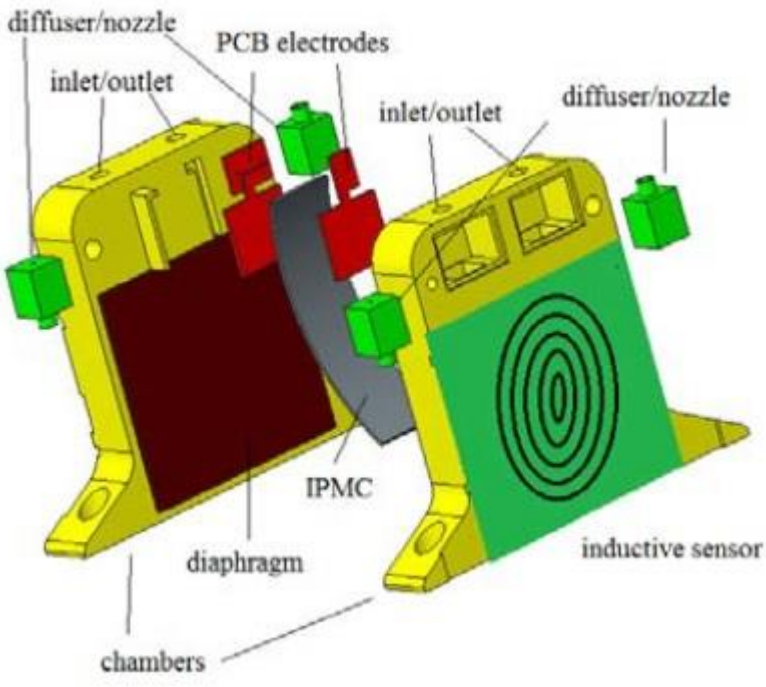

Figure 2.9: Pump structure (Jiaqi et al., 2016)

2.3.2 Microgrippers

For bio-micromanipulation tools, it is often carried out in a wet environment, and hence, IPMC is the promising candidate due to its wet environments tolerance. In addition, cells, bacteria and embryos are flexible and fragile object; hard finger microgrippers with large force exerted could have damage on such objects. Therefore, the flexible and biocompatible properties have elevated IPMC to be a popular candidate in micromanipulation applications. (Jain et al., 2011) and (Deole et al., 2008) presented the IPMC-based microgripper for pick-and-place operation. These microgrippers presented gripping motion with two identical active fingers, clamped with external holder. However, according to (Ford et al., 2014), the alignment effort of the two fingers upon activation is a formidable task. Therefore, Ford et al.

proposed a single activated IPMC-based microgripper that performs gripping motion by one actuating finger and one stationary finger. However, the reported microgrippers utilize external clampers that further increase the size. In addition, the mobility of the devices is severely constrained by the need of wired interface.

2.3.3 Surgical Tools

IPMC actuation can mimic biological muscles which make the actuator fit for advanced biomedical and surgical robotics. For example, (McDaid et al., 2012) reported a surgical robotic to control surgical instrument such as forceps and scalpel with IPMC actuator attached at each joint of the robotic arm. Besides, (Lin et al., 2009) reported an active catheter surgical tools with the curvature tip controlled by the IPMC actuator. The experimental characterization shows good results for the targeted applications with accuracy and fails safe compliance. The IPMC movement was controlled by using an adaptive controller such as PID and LPV.

2.4 Concluding Remarks

The fundamental theory of IPMC and the WPT via magnetic resonant coupling has been studied in this chapter. IPMC is chosen as the actuator in this project based on the advantages of low driving voltage, high efficiency and simplicity of fabrication. The magnetic resonant coupling is chosen as the

wireless powering scheme for the IPMC actuator as it is a promising candidate for size, safety, distance and efficiency issue.

CHAPTER 3

PLANAR-BASED WIRELESS MAGNETIC RESONANT COUPLING POWER TRANSFER SYSTEM

3.1 Introduction

IPMC is an EAP that can be actuated at very low drive voltage, fast response and ease of miniaturization as discussed in Chapter 2. It is highly attractive as biomedical device due to its soft muscle-alike and biocompatible properties (Fang et al., 2007). In this project, a planar-based WPT system via magnetic resonant coupling scheme is designed, fabricated and characterised. The resonant frequency and S_{11} parameters of the LC receiver circuit in different mediums were experimentally analysed. The interaction behaviour between the transmitter and receiver circuits is also experimentally examined.

3.2 Design and Working Principles of Planar-based Wireless Magnetic Resonant Coupling Power Transfer System

Figure 3.1 shows the design and working principles of the planar-based WPT system via magnetic resonant coupling. The system involves a LC transmitter and receiver circuits, which was designed to have two square-spiral coils as the resonator and source or load loops, respectively with integrated capacitor plate to form LC resonant circuit. The load loop induces the AC

voltages when the receiver exposed to magnetic field produced by transmitter circuit when the field frequency matches its resonant frequency, as discussed in preceding chapter. To control IPMC in unimorph motion, the LC receiver circuit is coupled with a class-D half wave rectifier circuit (Kkelis et al., 2015). The lumped mass model of the resonant coupling system is shown in Figure 3.2, where the L_1 and L_2 represent the source loop and resonator of transmitter circuit, respectively, and L_3 and L_4 represents the load loop and resonator of receiver circuit, respectively. The induced AC voltage from the LC receiver is converted into DC voltage via rectifier circuit to power up the IPMC actuator. Table 3.1 shows the parameter representation and the calculated components values using the *Modified Wheeler formula* and capacitance formula. The resonator of the transmitter and receiver are resonantly coupled and the resonant frequency is obtained by tuning the shunting capacitor C_1 and C_2 based on the following equations:

$$\frac{1}{L_2 C_1} \approx \frac{1}{L_3 C_2} \tag{3.1}$$

To enhance the transmission distance between the transmitter and receiver circuit as discussed in (Cheng et al., 2016), the diameter of resonator in transmitter circuit (100 mm) is designed to be larger than the receiver circuit (13 mm). The transmission distance, D is then estimated through the expression:

$$D = \sqrt{D_{0\_Tx} D_{0\_Rx}} \tag{3.2}$$

where D_{0_Tx} is the diameter of the resonator in transmitter circuit and D_{0_Rx} is the diameter of the resonator in receiver circuit. The resonant frequency of the WPT system is designed at 25 MHz with the estimated maximum transmission distance of ~5 cm. The IPMC actuator bends at resonant frequency due to the migration of mobile cations to the negative side (cathode) in the ion exchange membrane.

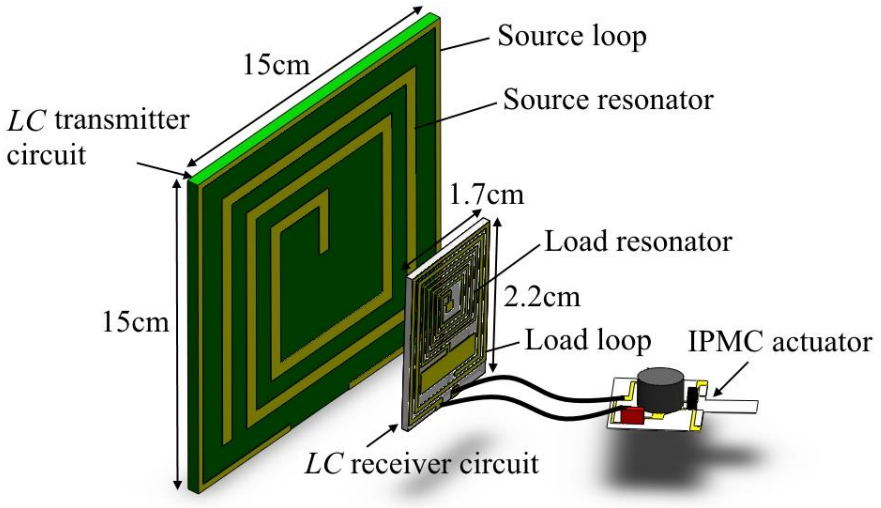

Figure 3.1: Design and working principle of the planar-based WPT

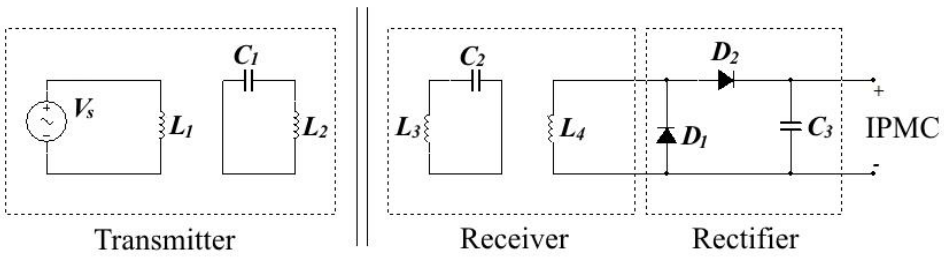

Figure 3.2: Lumped mass model of the resonant coupling system

Table 3.1: Parameter of the WPT system

Parameter	Representation	Value
Vs	AC Voltage input	15 Vac
L1	Source loop inductance	2503.176 nH
L2	Source resonator inductance	1791.462 nH
L3	Load resonator inductance	1482.834 nH

Parameter	Representation	Value
L_4	Load loop inductance	151.962 nH
C_1	Source capacitor	23.053 pF
C_2	Load capacitor	27.85 pF
C_3	Rectifier capacitor	220 μF
D_1	Rectifier diode	n/a
D_2	Rectifier diode	n/a

3.3 Fabrication of Planar-based Resonant Circuit

The planar-based LC receiver and DC rectifier circuit were fabricated from a double sided and single sided Cu-clad PI films (AP7156E, DuPont, USA) via dry film photolithography process, respectively. Figure 3.3 illustrates the fabrication process for LC receiver and DC rectifier circuits. The photolithography for the LC receiver fabrication was performed with dry-film photoresist. First, both top and bottom sides of the LC receiver circuit were fabricated by wet etching of the Cu-clad layer using a patterned photoresist as the mask (Figure 3.3(i-iii)). Next, to make a connection between top and bottom Cu side of the film, vial contact were etched at the PI film and covered with silver conducting epoxy. The fabricated LC receiver circuit is shown in Figure 3.4. The similar fabrication method was applied to fabricate the 0.11 mm thick DC rectifier circuit with bonded power electronic components to form class-D half wave rectifier circuit, as elucidated in Figure 3.3(iv-vi).

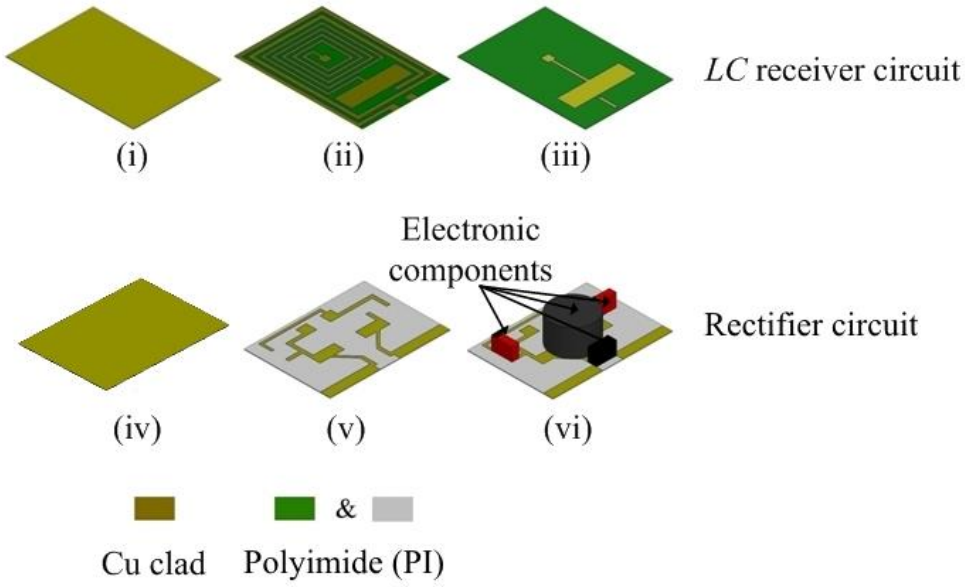

Figure 3.3: Planar-based WPT fabrication process. (i) double layer Cu-clad sheet, (ii) forming of inductor and capacitor plate (top view), (iii) forming of capacitor plate (bottom-view), (iv) etching of the rectifier circuit, (v) soldering of the electronic components and (vi) bonding the IPMC cantilever with rectifier circuit

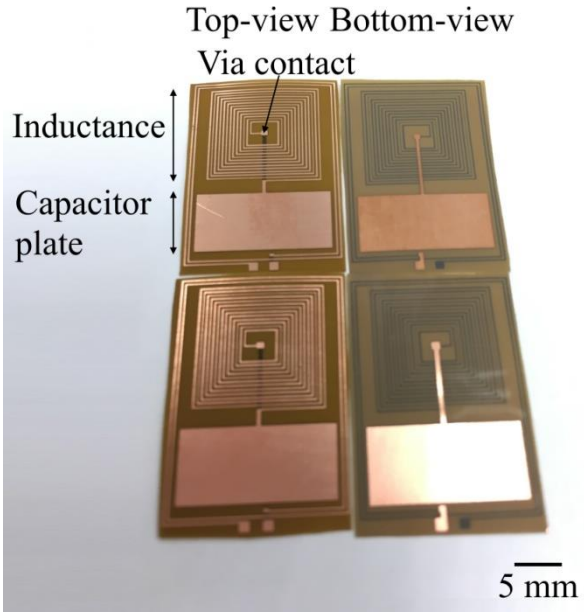

Figure 3.4: Top and bottom view of the fabricated LC receiver circuit

3.4 Results and Discussion

This section reports the characterization and experimental results for the wireless power transfer of the fabricated planar-based LC receiver circuit including the measurement of its resonant frequency, coupling effect and the interaction behaviour between transmitter and receiver.

3.4.1 Experimental Setup

To demonstrate the proposed wireless magnetic resonant coupling power transfer system, the experimental setup in Figure 3.5(a) and Figure 3.5(b) were constructed. A square wave function generator (SFG-830, GW Instek, Taiwan) and an op-amp amplifier (output power of 0.6 W) were implemented to produce magnetic field with the LC transmitter circuit connected. An oscilloscope (MDS1102CA, Matrix, China) was used to determine the electrical response of the LC receiver circuit and DC rectifier circuit.

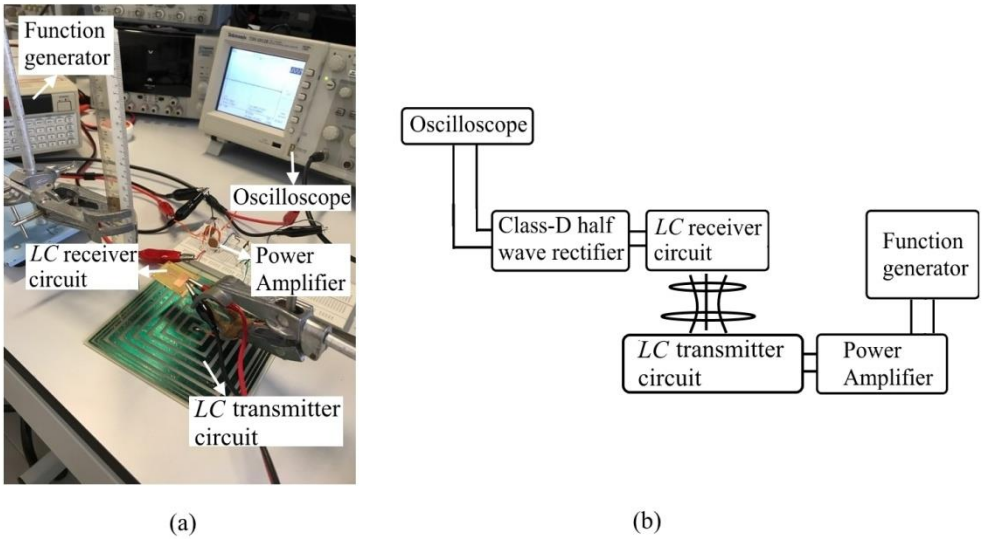

Figure 3.5: Experimental setup (a) transmitter and receiver setup and (b) block diagram of whole setup

3.4.2 Resonant Frequency

The constructed wireless power transfer system was designed to be operated at ~25 MHz, based on the tunable value shown in Table 3.1. To feature biocompatibility of the developed LC receiver circuit, the LC receiver circuit was encapsulated with a layer of ~0.02 mm thick polydimethylsiloxane (PDMS) material. Figure 3.6 illustrates the induced DC output voltage at the DC rectifier circuit with the LC receiver circuit without PDMS encapsulation (direct exposed to air) and with PDMS encapsulation. A maximum DC output voltage of ~2.3 Vdc was noted in both cases at the same resonant frequency, ~25 MHz. This shows that the PDMS medium does not cause significant change in the device's resonant frequency. In addition, it also shows a good agreement with the theoretical calculated value, where a maximum output voltage is attained at resonant frequency of 25 MHz. To determine its resonant

frequency, S_{11} parameter measurements of LC receiver circuit, a Vector Network Analyzer (VNA) (Rohde & Schwarz, Germany) was utilized (see Figure 3.7, for measuring setup). To evaluate the effect of working environment on the resonance (see Figure 3.8, for experiment setup), the LC receiver circuit covered with PDMS was tested in DI water, air and skin mimicking gels (with and without muscle and fat gel models). The resonant frequency in these mediums exhibits almost identical response while different values of phase dip (Figure 3.9) are observed in water and air mediums. The PDMS encapsulation of the LC receiver circuit isolates the LC coil from the operating mediums (Abid et al., 2017) and hence, maintaining its inductance values; in comparison with the device reported by (Zainal et al., 2017), with their resonant frequency shifted when operated in water and air mediums. The difference of the phase dip in water and air mediums might due to the power absorption in water medium is higher than air medium (Geist et al., 2007). This test proves that the fabricated LC receiver circuit is well fitted for implantable purpose to work at different mediums.

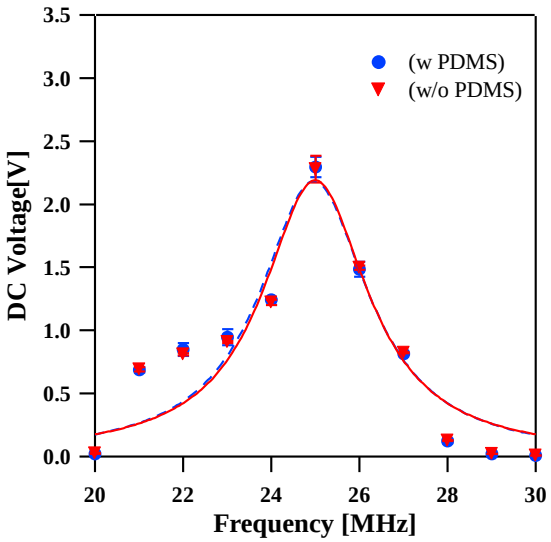

Figure 3.6: DC voltage at the rectifier circuit with LC receiver circuit without PDMS encapsulation and with PDMS encapsulation

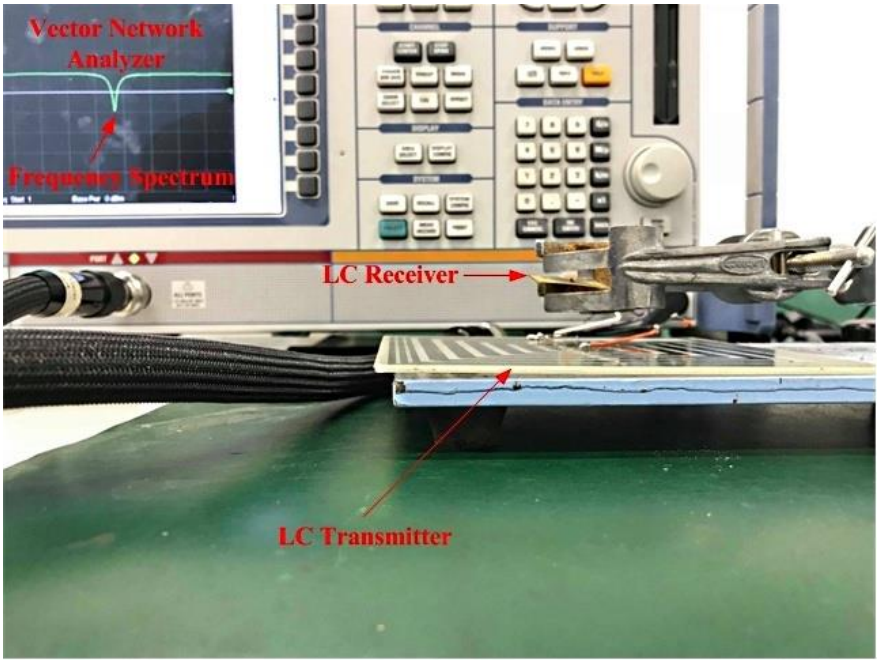

Figure 3.7: Experimental setup for resonant frequency characterization using S_{11} parameter. The LC receiver circuit was connected to the vector network analyzer and wirelessly measured through inductive coupling with a LC transmitter circuit

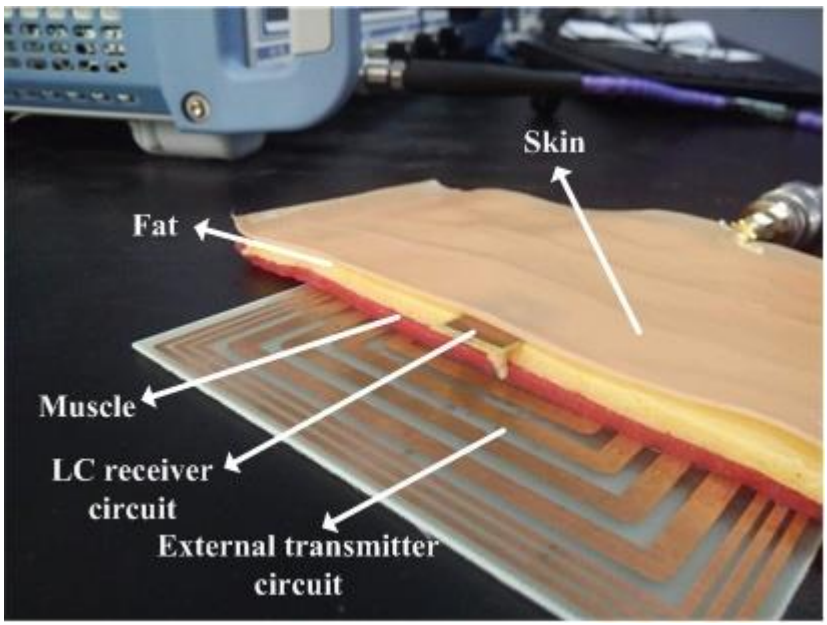

Figure 3.8: Experimental setup for measuring S_{11} parameters of the LC receiver circuit in a skin mimicking gels (with and without muscle and fat gel models)

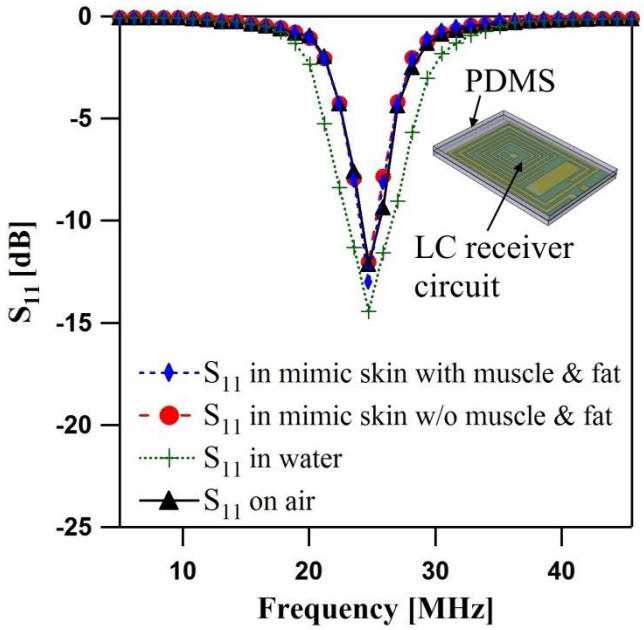

Figure 3.9: S_{11} parameter of the LC receiver circuit in air, water and skin mimicking gel (with and without muscle and fat gel models)

3.4.3 Coupling Effect of Transmitter and Receiver

The voltage output voltage of the LC receiver circuit also depends on the coupling mechanism with the transmitter circuit. To enhance the transmission distance and mobility coverage, the size of the transmitter coil is designed to have large dimension to enhance the wireless power transfer efficiency. Therefore, experiments were conducted to study the behaviours of the output voltage of the LC receiver circuit (after fed to the DC rectifier circuit) at different placement positions on the transmitter circuit which has 1.5 cm receiver-transmitter separation distance. Figure 3.10 shows the LC receiver circuit achieves large voltage response, ~2.9 Vdc when it is placed at the centre of the transmitter circuit and the voltage decreases when the LC receiver circuit shifts away from centre of the transmitter circuit.

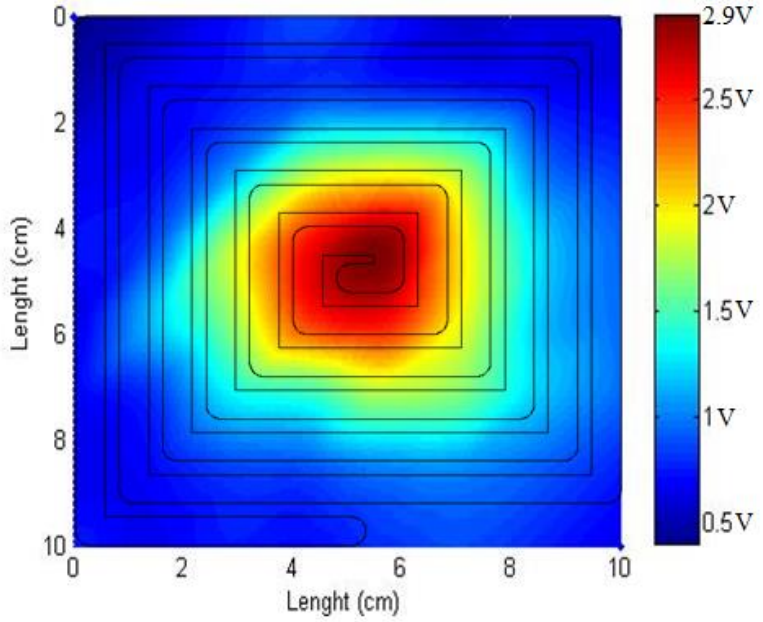

Figure 3.10: Coupling response of the LC receiver circuit due to different placements on the transmitter at 1.5 cm separation distance (after fed to a DC rectifier circuit)

3.4.4 Distance and Angle Characterization

Understanding the interaction behaviours between transmitter and LC receiver circuit is of importance to ensure optimum power transfer. In light of this, the maximum power transfer distance and the orientation of the LC receiver circuit were evaluated. The result presented in Figure 3.11 shows a gradually decrease of DC voltage when the distance between the LC receiver circuit and transmitter slowly increases, due to the reduction of the magnetic cutting. The losses of the magnetic flux have lead to the reduction of the power transfer efficiency between the transmitter circuit and LC receiver circuit. This result suggests that the maximum separation distance between the transmitter circuit and LC receiver circuit is 4.5 cm to produce the output voltage of ~1 Vdc (minimum voltage to activate the IPMC-based cantilever).

Figure 3.12 shows the response of the LC receiver circuit at different alignment angles where maximum voltage is noted at parallel alignment (0 degree from the transmitter) with the measured value of ~3.1 Vdc. This trend is consistent with the result of the maximum separation distance that is highly dependent on the magnitude of the cutting flux. There is no cutting of magnetic flux when the LC receiver circuit is placed in perpendicular to the transmitter circuit. Also, the magnetic flux produced losses in air have drag down the wireless power transfer efficiency of the transmitter and LC receiver circuit. It is worth nothing that, our developed prototype achieves 81% of power transfer efficiency, which is higher than the reported wireless powering devices (Cannon et al., 2009, Kurs et al., 2007, Abdelnour et al., 2012), with the range of 40 % to 60 %. Distance and angle between the transmitter and receiver may lead to the change of leakage inductance. The change of leakage inductance might result in the change of resonance frequency. Figure 3.13 examines the resonant frequency of the LC receiver circuit at different distance with the transmitter circuit. The resonant frequency remains constant with the phase dips increase when the distance between the transmitter circuit and LC receiver circuit increases. This result verified the voltage response of the LC receiver circuit. Figure 3.14 shows the resonant frequency of the LC receiver circuit at different tilting angle with the transmitter circuit. The coupling effect reduces when the angle is tilted away from 180º, which is illustrated in Figure 3.12. Therefore, the S_{11} magnitude in Figure 3.14 gradually increases when the tilting angle varies from parallel to perpendicular orientation. It is worth noting that the small leakage of the inductance does not affect the resonance frequency of the wireless power transfer system.

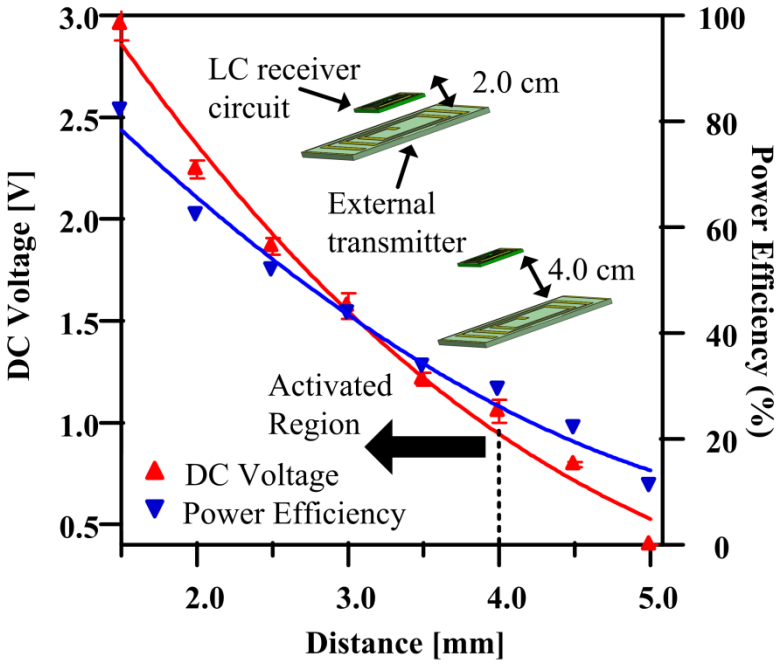

Figure 3.11: DC voltage versus distance between LC receiver circuit and external transmitter circuit

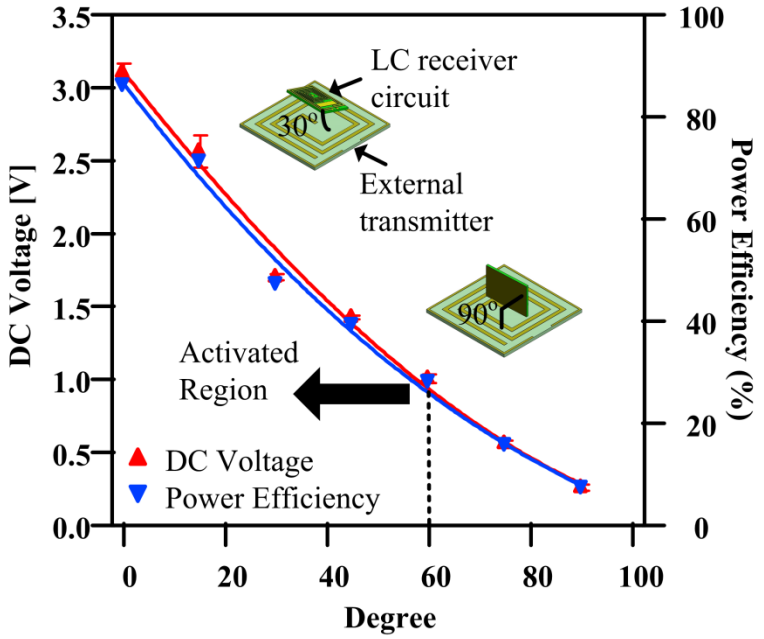

Figure 3.12: DC voltage versus tilting angle of LC receiver circuit

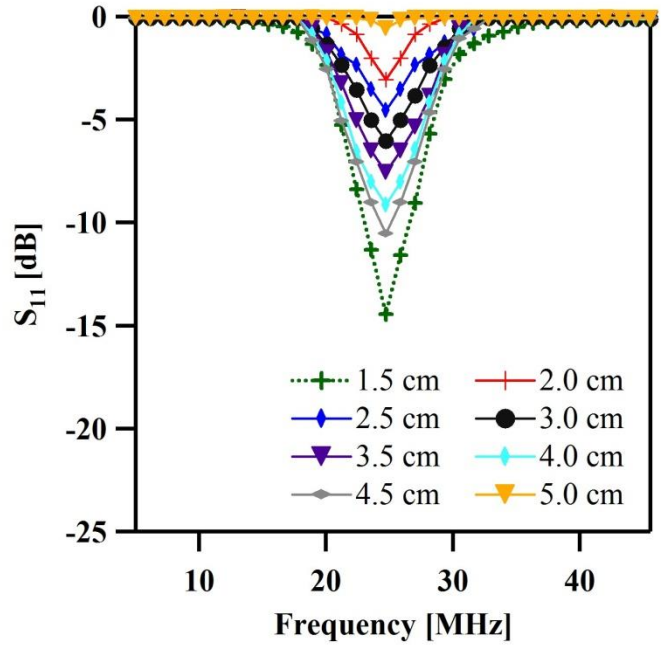

Figure 3.13: Resonant frequency versus distance between LC receiver circuit and external transmitter circuit

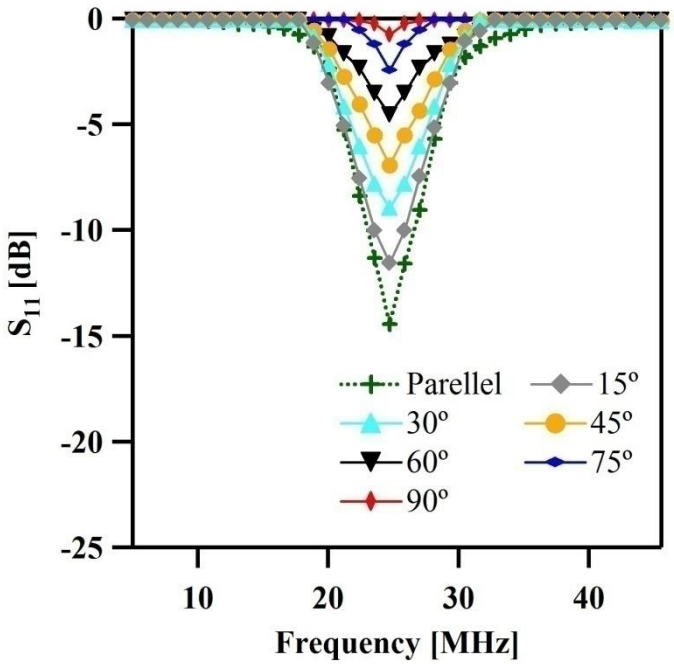

Figure 3.14: Resonant frequency versus tilting angle of LC receiver circuit

3.5 Conclusion

In this chapter, a wireless magnetic resonant coupling power transfer system has been designed, fabricated and demonstrated. The planar-based LC receiver circuit and DC rectifier circuit have been constructed to miniature the size of the whole antenna. The resonant characteristic of the fabricated LC receiver circuit with PDMS encapsulated has been tested in different mediums to prove that it is well-suited for implantable purposes to work at different mediums. The wireless coupling effect of the developed LC receiver circuit at different placement positions on the transmitter circuit was examined and analysed to enhance the performance of the wireless power transfer efficiency. Maximum voltage response, ~ 2.9 Vdc is reported when the LC receiver circuit is placed at the centre of transmitter. The distance and angle interaction between transmitter and receiver were evaluated to ensure optimum power transfer. ~0 Vdc obtained at LC receiver circuit when the distance is increased to maximum transmission distance of 4.5 cm, where maximum voltage is produced when the angle of LC receiver is parallel with the transmitter circuit.

CHAPTER 4

WIRELESS-POWERED IPMC-BASED MICROGRIPPER

4.1 Background

This chapter discusses the wireless powered IPMC for soft robotic microgripper application. The microgripper is passively controlled through wirelessly power transfer from the LC resonant circuit. The microgripper is designed to operate with one active finger and one stationary finger to eliminate misalignment issues. The gripping operation is performed by moving an active finger (made of IPMC actuator) to another stationary finger (made of Cu-clad PI sheet). The wireless responses of the microgripper are experimentally characterized. As a proof of concept for biomedical application, fish egg gripping was performed wirelessly using the fabricated device for demonstration purposes to represent the biological cell manipulation application.

4.2 Design and Working Principle of IPMC-based Microgripper

The developed wireless powered IPMC microgripper is operated by planar LC receiver circuit and DC rectifier circuit (demonstrated and characterized in Chapter 3) to control the single IPMC-based finger unimorph motion, as shown in Figure 4.1. The IPMC finger actuator is bonded to the DC

rectifier circuit fabricated from the Cu-clad PI sheet. The Cu-clad PI sheet which poses biocompatibility property as discussed in Chapter 2 also serves as a stationary finger. A copper hinge joint is created as a mechanical support to have a more rigid surface to facilitate object gripping. Compared to (Ford et al., 2014) that utilizes external hard steel sheet as the stationary finger, this approach is merited from simple and small size features. The distance between both active and stationary fingers can be customized to cater for different objects gripping sizes. In this work, the distance between the fingers is selected as 1.5 mm to accommodate a fish egg's size. To activate the IPMC finger, an AC current is induced in the LC receiver circuit (consist of resonator and load loops) when it is exposed to external AC magnetic field through the electromotive force that is generated by the external transmitter when the external frequency matches the resonant frequency of the LC receiver circuit. The induced AC current is rectified into DC signal through rectifier circuit to activate the IPMC finger. The IPMC finger bends towards the stationary finger when the DC is raised above the cut off voltage, V_m, to perform a gripping action, due to the migration of mobile cations in the ion exchange membrane (Nafion polymer) towards the electrodes (Shahinpoor and Kim, 2001) (Refer Figure 4.2). The bending displacement can be controlled wirelessly by manipulating the voltage of the LC receiver circuit. This feature offers an advantage to control the holding force of an object. Finite element tool, COMSOL Multiphysics^{TM} was used to make a deflection analysis of the IPMC based actuating finger. The result of the analysis suggests a suitable dimension of device to promise that the IPMC-based actuating finger provides sufficient displacement. The simulation result in Figure 4.3 shows the

maximum tip displacement of 0.7 mm at time 0.6 s. This is obtained by evaluating the time response of the IPMC active finger when 3 V_{DC} was applied to it.

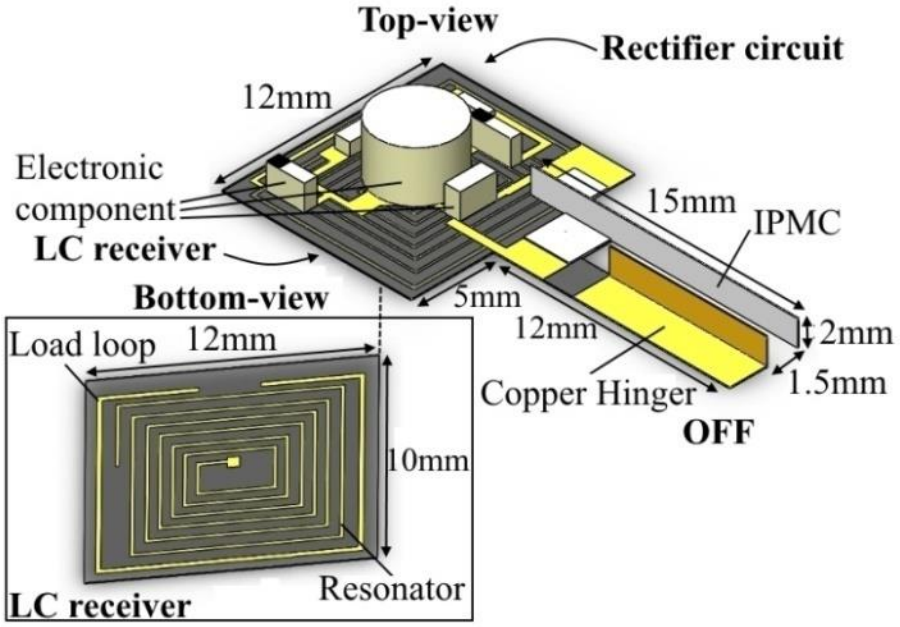

Figure 4.1: Top and bottom view of device

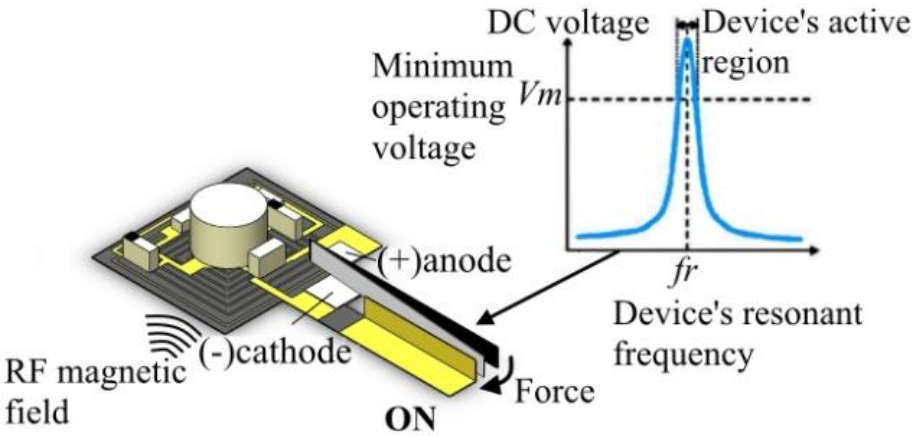

Figure 4.2: Device conceptual diagram

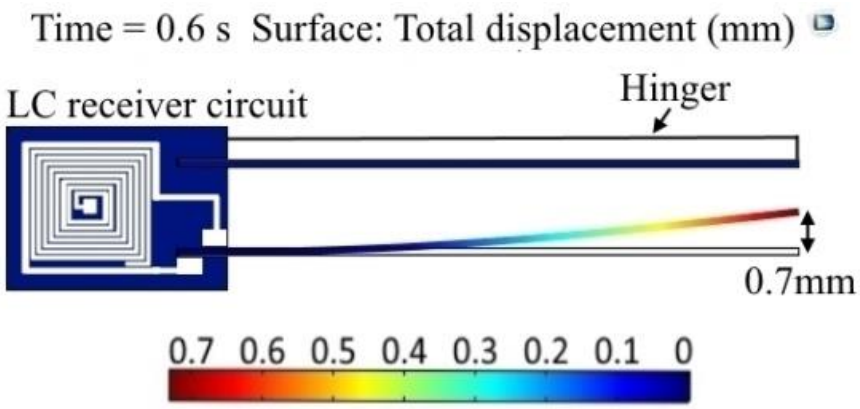

Figure 4.3: COMSOL simulation model of the device with IPMC actuator showing approximate displacement of 0.7 mm

4.3 Fabrication of IPMC-based Microgripper

The wireless activated microgripper developed in this work comprises LC receiver circuit, and a class-D DC half wave rectifier circuit integrated with a single active IPMC-based finger with the length of 15 mm and height of 2 mm. The planar LC receiver circuit and DC rectifier circuit were fabricated using double sided Cu-clad PI sheet with 9 μm-copper thickness at the bottom and top polyimide surface respectively same as described in Chapter 3. Photolithography was performed for the fabrication of the both LC receiver and DC rectifier circuits with dry-film photoresist. These circuits were developed by wet etching the copper layer with a patterned photoresist as the masks (Figure 4.4(a-b)). After that, the vial contacts were formed to make an electrical connection between the LC receiver (bottom layer) and DC rectifier (top layer) circuits. Electronic components were then soldered on the top layer to complete the DC rectifier circuit (Figure 4.4(c)). The stationary finger was fabricated by folding the copper clad polyimide 90 degree to create hinge joint for stiffer structure. The IPMC based actuating finger was fabricated from

Nafion-117 with 183 µm thickness and the electrodes were plated using the deposition metal electrode method as discussed in Chapter 2. Firstly, the Nafion-117 membrane was cut into desired dimension, then following by blasting process to increase the surface area density of the electrodes. Then, the processed membrane was cleaned by using de-ionized water and mixture of H_2SO_4 and H_2O_2. To pattern the cleaned Nafion-117 with two electrode designs (anode and cathode), photolithography process was applied. Next, the Nafion-117 was immersed into $[Ag(NH_3)_2]OH$ complex solution with the additional of 0.8 g glucose to form silver electrodes on both surface (chemical reaction details can refer to Chapter 2). Finally, the developed IPMC-based finger was bonded to the DC rectifier circuit using silver conducting epoxy and was cured at room temperature for 15 minutes (Figure 4.4(d)). The complete fabricated device and the LC receiver circuit are shown in Figure 4.4(e).

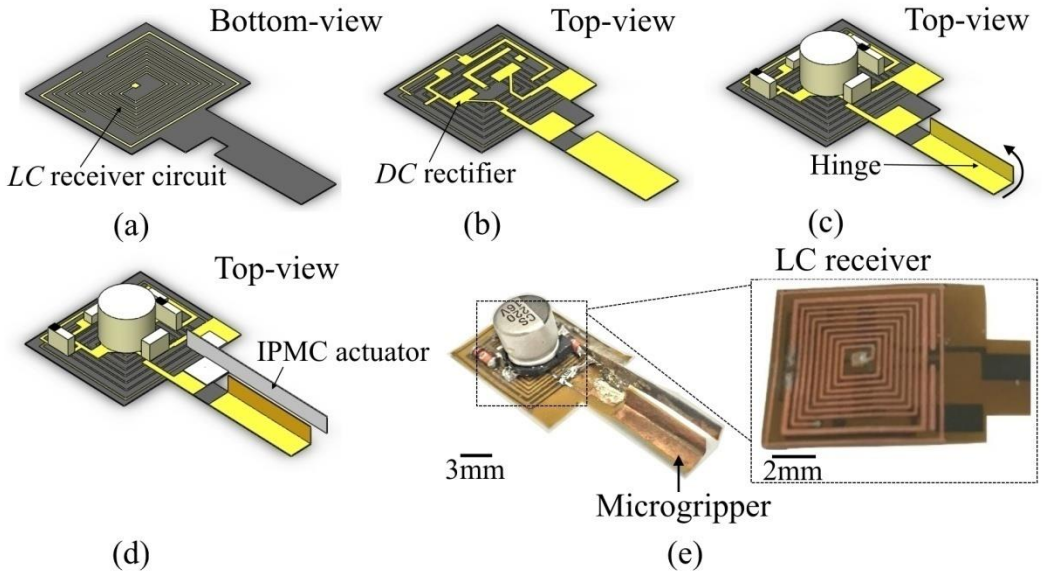

Figure 4.4: Device fabrication process (a) etch Cu of LC receiver circuit, (b) etch Cu of DC rectifier circuit, (c) electronic component soldered and hinge joint created, (d) bond IPMC actuator with DC rectifier circuit using silver epoxy, and (e) complete device

4.4 Experiment Results and Discussion

The characterization and experimental results for the IPMC-based finger and the fabricated microgripper are presented in this section. The performance of the device is evaluated through wireless actuation test. Fish egg gripping experiment was carried out wirelessly using the device as a proof of concept toward biological cell manipulation application.

4.4.1 Experimental Setup

Wireless experiments for the fabricated device were performed using the similar setup as illustrated in Chapter 3, composing of square wave function generator (SFG-830, GW Instek, Taiwan) and class-E power amplifier (output power of 0.65 W) that were implemented to produce magnetic field with transmitter connected to the amplifier. An oscilloscope (MDS1102CA, Matrix, China) was used to determine the electrical response of the LC receiver circuit and DC rectifier circuit. The setup in this case involved a laser displacement sensor (CD5-85, Optex, Japan) and weight balancer to characterize the displacement and force of the active finger caused by the soft IPMC actuator, respectively. Figure 4.5 illustrates the experimental setup that is utilized in this case. The wireless gripping tests were conducted by gripping the fish egg in a petri dish filled with DI water that located above the transmitter circuit. The gripping motion was recorded using USB digital microscope (Dino-lite, Taiwan) and activated the wireless microgripper by externally radiating an RF field from the transmitter.

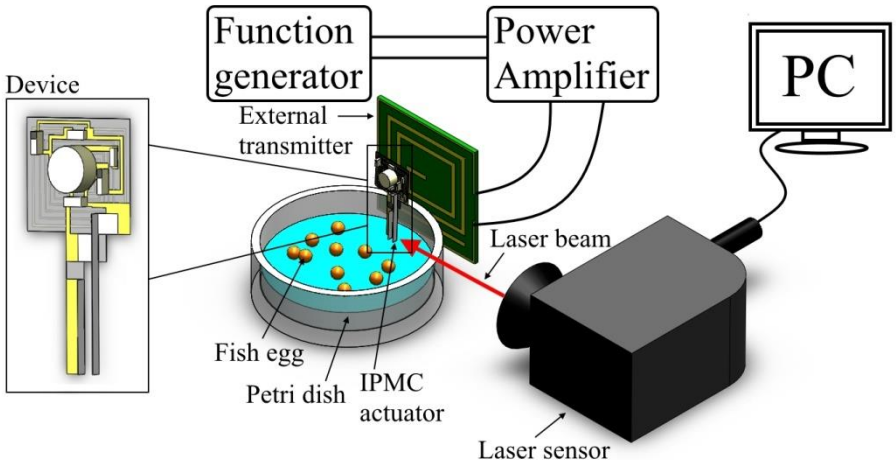

Figure 4.5: Experimental setup for wireless demonstration

4.4.2 IPMC Finger Characterization under Wireless Configuration

The device's LC receiver circuit was designed to be operated at 13.56 MHz, based on the tunable *LC* values (resonator's loop L = 417 nH and C = 330 pF) in the LC receiver circuit. Hence, the wireless activation of the active microgripper was performed when the field frequency generated by transmitter matches with the resonant frequency of the LC receiver circuit (13.56 MHz at a constant output power of 0.65 W). The gripping force characteristic of the developed microgripper was studied to ensure it has sufficient energy to grip an object. Experiment was performed using a mass balance by converting the mass value into force. The IPMC was activated in the 10th seconds with 3 V_{DC} supplied from the LC receiver circuit. Figure 4.6 shows the temporal response of the tip forces of the IPMC finger increases dramatically upon wireless activation with the maximum recorded value of 0.17 mN. The IPMC finger shows a rise time of 13 s before reaching steady-state response. Small measurement is noted prior to the wireless actuation and

this may be contributed by the environment noise such as uniform air flow. To experimentally access the microgripper bending behaviour at different activation cycles, the external transmitter was tuned in three set of ON/OFF cycles: 10 s ON, 20 s OFF with 3 V_{DC} supplied voltage, shown in Figure 4.7. Figure 4.7 shows the voltage induced at the LC receiver circuit is linearly corresponding to the temporal response of the IPMC gripper's displacement at the 10th second of 1st set activation cycle with the noticeable deflection of 0.26 mm. At the OFF cycle, the voltage level at the LC receiver circuit drops to 0.8 V and the IPMC gripper maintains at 0.26 mm. This behaviour repeated for 2nd and 3rd cycle sets of the experiment. The 2nd and 3rd set continues from end of the OFF-state of the previous cycle, with the measured value of 0.46 mm and 0.57 mm, respectively. The rise time of the IPMC gripper's displacement shows an increasing trend, with the measured value of ~9 s, ~7 s and ~4.3 s, respectively at 1st, 2nd and 3rd cycle sets. A possible reason for this phenomenon is the moving cations in the IPMC gripper do not migrate back to its original position due to the absence of potential difference at the OFF cycle. This experiment shows that the displacement of IPMC-based finger can be controlled in a step-wise form to grip an object in a more precise and accurate way. This actuation behaviour was further tested for three different IPMC samples at three ON-OFF cycles using the same experiment setup operated at 5 V_{DC}. Figure 4.8 shows the samples experience a close cumulative deflection value for each ON-OFF cycle, with the measured standard deviation of ~0.05 mm between the samples. The deviation might be due to different thicknesses of the silver layer plated on the Nafion membrane in which the conductivity of the electrodes were altered and hence, affecting

the performance of the IPMC actuator (Zhang et al., 2007). Despite this, the three samples presented show the increment of the displacement in the ON-OFF cycle (stepwise operation) with the cumulative measured values of 1.17 mm, 1.19 mm and 1.24 mm, respectively for 1st, 2nd and 3rd samples. In each of the tested sample, the subsequent IPMC actuator deflection decreases (~0.18 mm) as compared to the previous deflection at each stepwise activation cycle. This decrement is possible as the previous migrated cations in the IPMC actuator do not migrate back to its original position in the OFF cycle as mentioned above, and hence, the induced potential difference across the IPMC in the next activation cycle continues to migrate the remaining cations and redistribute their positions at the Nafion-117 membrane surface. In other word, less cations migrate to the electrode compare to the previous ON cycle.

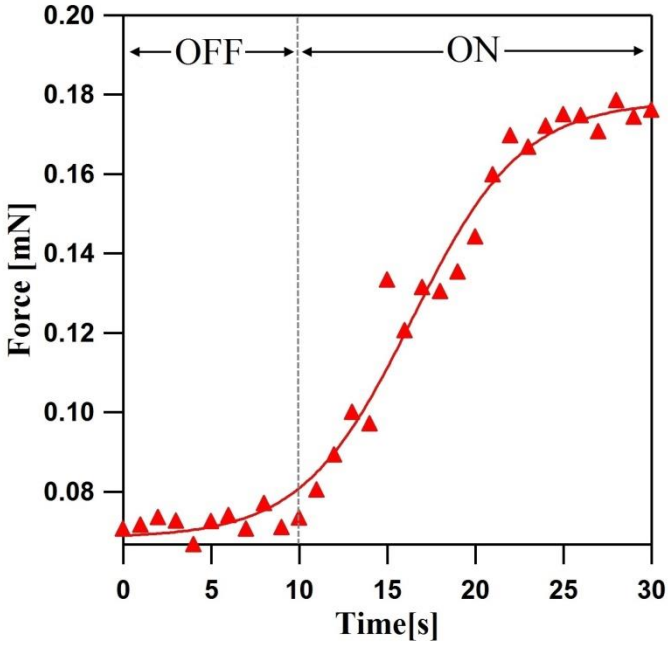

Figure 4.6: IPMC actuator tip force versus time at 3 V_{DC}

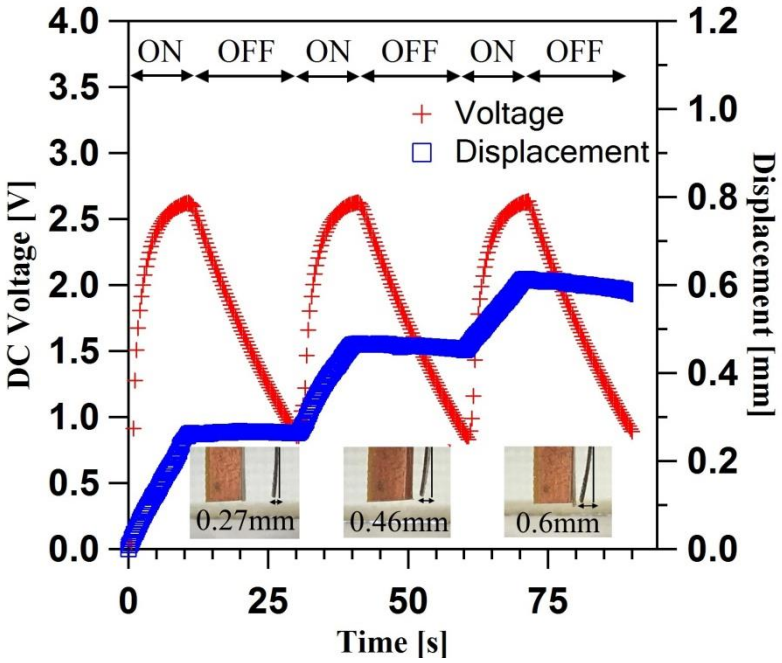

Figure 4.7: IPMC actuator tip displacement and DC voltage versus time at 10 s ON and 20 s OFF activation cycle

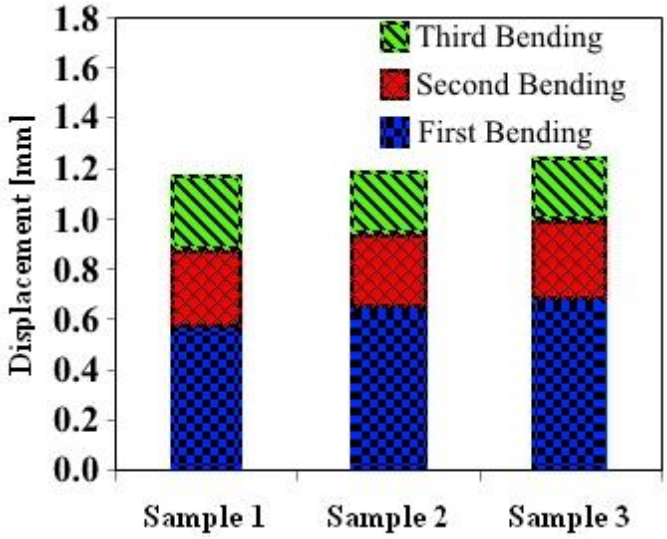

Figure 4.8: Three samples of IPMC actuators with 5 V_{DC} applied

4.4.3 Application of IPMC-based Microgripper

The proof of concept of the wireless powered soft microgripper in biological cell manipulation was demonstrated by gripping a fish egg. Fish egg

has been widely implemented as the test object in biological cell manipulation, as reported in (Wakimoto et al., 2011, Pillarisetti et al., 2005). The experimental setup used is shown in Figure 4.5. Figure 4.9(a) shows samples of fish eggs with average diameter of ~1 mm placed in petri dish with DI water. In Figure 4.9(b), the microgripper approaching the fish egg samples in an OFF mode. The microgripper was activated in Figure 4.9(c) with an external magnetic field with the field frequency of 13.6 MHz generated by the transmitter circuit. When the resonant frequency of the LC receiver circuit matches the field frequency, the IPMC based finger was activated and it gripped an fish egg in a unimorph motion. Figure 4.9(d) shows the release process of the fish egg by turning off the wireless transmitter. These results show that the IPMC-based finger perfectly grips the fish egg sample with sufficient holding force without causing any physical damage to the fish egg. This demonstrated the potential application of the developed soft microgripper for biological cell manipulation. It can be noted that the microgripper can be tuned to grip variable sized object by incorporating a switching circuit at the DC rectifier to change the polarity of the IPMC gripper and expand its opening gap when expose to different radio frequency range.

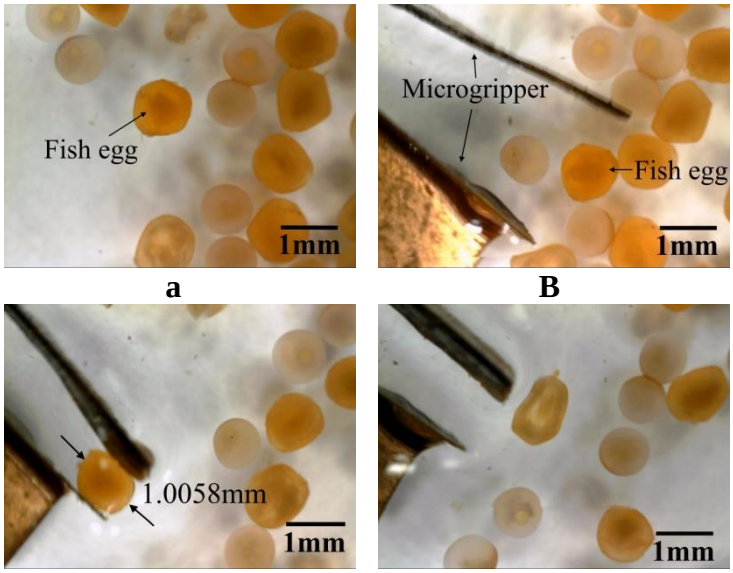

Figure 4.9: Wireless gripping fish egg demonstration using fabricated device (a) fish egg, (b) microgripper approaching to the fish egg, (c) the finger of the microgripper was closed to grip fish egg by tuning field frequency to device's resonant frequency ~13.61 MHz and moved the fish egg apart from the rest, and (d) fish egg released by tuning off the wireless transmitter

It is constructive to compare the performance of the developed soft microgripper with its counterpart reported in the literature. Table 4.1 summarizes the performance of reported IPMC soft microgripper based on their maximum deflection (mm) per unit IPMC area (mm^2) ratio. As compared to IPMC gripper demonstrated by (Jain et al., 2011), our work has slightly lower maximum deflection (mm) per unit IPMC area (mm^2) ratio due to transmission loss in wireless powering scheme. This constraint can be easily addressed by utilizing high frequency transmission range. On the other hand, when comparing to (Chattaraj et al., 2014) and (Bhattacharya et al., 2016), our work scores well with the maximum deflection (mm) per unit IPMC area (mm^2) ratio of $0.041\,(mm)^{-1}$ due to the small footprint of the IPMC microgripper. Moreover, compared with aforementioned microgripper, this

project develops integration effort where no external bulky clamper is needed to fix the IPMC microgripper while offering superb device mobility.

Table 4.1: Performance comparison with other IPMC based microgrippers

Authors	Maximum deflection	Area dimension (IPMC)	Deflection/ dimension	Powering scheme
(Chattaraj et al., 2014)	8.55 mm	225 mm^2	0.038	Wired
(Bhattacharya et al., 2016)	2.46 mm	244 mm^2	0.010	Wired
(Jain et al., 2011)	14.00 mm	240 mm^2	0.058	Wired
This work	1.24 mm	30 mm^2	0.041	Wireless

4.5 Conclusion

Wireless powered single finger activated microgripper using external RF magnetic field has been designed, fabricated and tested on a proof-of-concept biological cell manipulation with the fish egg gripping. A flexible polyimide LC receiver circuit was integrated with a soft IPMC finger to serve as the electroactive actuator, demonstrating the unimorph bending motion with the tuned frequency. The soft prototype fabrication is based on flexible polyimide manufacturing technology combined with silver mirror casting technique of the IPMC actuator. The wireless characteristic of the fabricated single finger activated microgripper shows a maximum deflection of 0.765 mm (activation force of 0.17 mN) at the RF power of 0.65 W with 3.5 V_{DC}, when the external field frequency matches the resonant frequency of integrated LC receiver circuit, ~13.6 MHz. A total cumulative of ~0.6 mm IPMC deflection was performed in a wireless stepwise operation at ~2.6 V_{DC} output voltage The total cumulative of the IPMC deflection were increased to 1.17 mm, 1.19 mm and 1.24 mm at 5 V_{DC} output voltage for three different

samples. The device successfully performs task on manipulating the fish egg sample which shows its potential opportunity towards the application as biological cell manipulator. Future works will encompass further improvement of the device design, including the wireless IPMC actuator for enhanced performance in device size and bending speed as well as the microgripper packaging with biocompatible material for further characterization of *in vivo* model.

CHAPTER 5

WIRELESS ACTIVATED DEVICE WITH INTEGRATED IPMC CANTILEVER VALVE FOR TARGETED DRUG DELIVERY

5.1 Background

Apart from the IPMC-based microgripper, this project also demonstrated a potential implantable IPMC-based drug delivery device, which allows drugs to be provided at efficacious location to maximize the effectiveness of drug therapies. The drug delivery device utilises a soft cantilever valve that is made of IPMC actuator controlled by an integrated planar LC receiver circuit through RF magnetic field. Under an applied voltage, the developed cantilever valve deflects to activate the drug release mechanism. The wireless test of the IPMC-based cantilever valve has been experimental characterized. To demonstrate wireless drug release, the fabricated device was loaded with dye solution and immerged into DI water and activated utilized RF magnetic field generated by the external transmitter circuit. Systematic in vitro study demonstrates the reduction of HeLa cell viability through the release of Cisplatin drug from the developed prototype. These results demonstrated the proof of concept of the wirelessly activated soft IPMC cantilever valve for mobile, reliable and safe targeted drug delivery.

5.2 Design and Working Principle of Drug Delivery Device

The design of the developed drug delivery device is depicted in Figure 5.1(a, b). The device body was made of biocompatible polydimethylsiloxane (PDMS) (Pirmoradi et al., 2011). It is designed to have overall dimension of 15 × 25 × 6 mm^3, including a drug reservoir with maximum loading capacity 520 μL. The wireless power transfer setup utilizes a planar inductor-capacitor (LC) resonant circuit that serves as the wireless receiver to activate the IPMC cantilever and an external transmitter circuit as discussed in Chapter 3. The LC receiver circuit consists of two rectangular-spiral coils as the resonator and load loops or source loops with integrated capacitor plates to form an LC tank, fabricated using printed circuit board technology.

The LC tank is coupled with a DC rectifier circuit, fabricated from a single-sided copper-clad polyimide (PI) film with 0.11 μm thickness. The LC receiver circuit is encapsulated at the bottom of the device body with 0.1 mm thick PDMS layer. A square cavity is created at the pump body to accommodate a DC rectifier circuit with integrated IPMC-based cantilever to function as a wireless valve to control the opening gap over the release orifice of the drug delivery device.

Operation of the device is controlled by wirelessly resonating the LC tank. The load loops induce an AC voltage through faradays law,(Mousavi et al., 2018) when it is exposed to the external magnetic field generated by the

external transmitter circuit at its resonant frequency. The cantilever bends when the induced DC voltage from the DC rectifier circuit rises above a critical value, due to the migration of mobile cations in the IPMC material to the cathode, as shown in Figure 5.2(a). This phenomenon creates a pressure across the cantilever and bends it toward the anode.(Shahinpoor and Kim, 2001) This deflection opens the release orifice and creates pressure inside the reservoir to pump the drug out. The rate of drug release can be wirelessly controlled by manipulating the bending force through tuning the RF input power from the external transmitter. Increasing the RF power increases the bending displacement of the IPMC-based cantilever, leading to a larger pressure induced.

An analysis using COMSOL Multiphysics optimized the design dimension to provide sufficient displacement to move the valve away from the release orifice. The numerical model can predict the displacement and the temporal response of the IPMC-based cantilever valve. Figure 5.2(b) shows a maximum displacement of 0.11 mm with an applied DC voltage of 2 V.

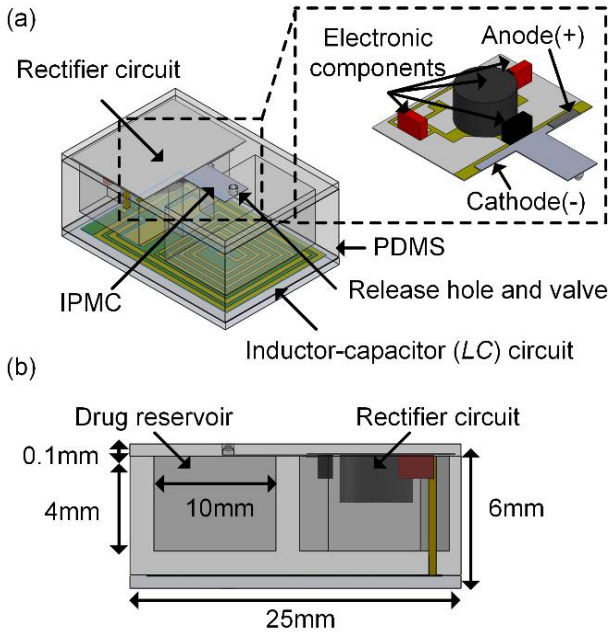

Figure 5.1: IPMC-based cantilever valve for drug delivery (a) schematic illustration of the drug delivery device, and (b) Side-view of the device

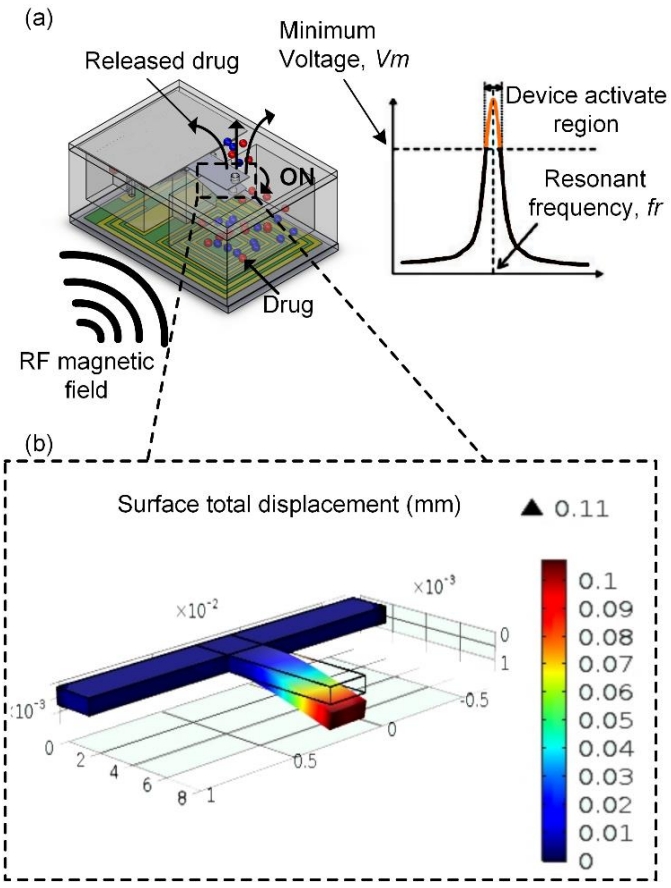

Figure 5.2: (a) Conceptual diagram and frequency-sensitive working principle of the device, and (b) simulation result of the IPMC-based cantilever using COMSOL Multiphysics

5.3 Fabrication of IPMC-based Drug Delivery Device

The construction of the drug delivery device followed three main steps, i.e., LC circuit fabrication, integration of the IPMC cantilever to the fabricated DC rectifier circuit and the fabrication of the pump body. Figure 5.3(a) shows the fabrication and integration processes for the fabrication of the drug delivery device. LC circuit fabrication was using process discussed in previous chapter. First, a double sided Cu-clad PI film (AP7156E, DuPont Pyralux Polyimide Film, USA) was patterned with two rectangular-spiral coils as the resonator and load loop and a capacitor plate via dry film photolithography process. Next, both top and bottom sides of the LC receiver circuit undergo etching process to remove the copper-clad layers. Vial contacts were etched at the PI film and sealed with silver conducting epoxy to connect the top and bottom copper side of the PI film. Subsequently, a 0.11-mm thick DC rectifier circuit was fabricated using the similar method, with bonded power electronic components to form class-D half wave rectifier circuit. The fabricated IPMC was cut into T-shape to form a 8-mm long cantilever and bonded to the DC rectifier circuit. The electrical contact between the LC receiver circuit and DC rectifier circuit was achieved using silver conducting epoxy. Both circuits were coated with polydimethylsiloxane (PDMS) layer (Sylgard 184, Dow Corning Corp, USA) (mixed with the ratio of 1: 10) to make the surface electrically isolated and biocompatible.

The IPMC-based cantilever valve was fabricated from Nafion-117 film (Dupont, USA) of 183 µm thickness detail of the process were reported in Chapter 2. However, the chemical electroless plating might induce high internal stress to the IPMC and result to serious curliness. Therefore, low temperature annealing was performed to remove the internal stress. The IPMC cantilever was placed in a vacuum drying oven and heated at 140 °C for 3 hours. Figure 5.4 shows the IPMC cantilever after the annealing process. The IPMC cantilever is flattened due to the removal of internal stress. Finally, the developed IPMC cantilever was bonded to the DC rectifier circuit using silver conducting epoxy. Later, the pump body was constructed by pouring the same PDMS solution to a 3-D printed mold (using B9 creator, USA) and cured at room temperature for 48 hours. Finally, the LC receiver circuit and DC rectifier circuit were bonded to the constructed pump body with a punched 1-mm release orifice. The LC receiver circuit is integrated as a wireless receiver into the IPMC-based cantilever using chemical deposition on the photo lithographically patterned Nafion 117. The process forms different polarity electrode pads and is bonded to the DC rectifier. This technique allows for a small device footprint, in contrast to the previously reported bulky devices with external clamps as electrode.(Ford et al., 2014) Figure 5.3(b) shows the fabricated drug delivery device and the scanning electron microscopy (SEM) image of the fabricated IPMC-based cantilever with the silver electrode layer.

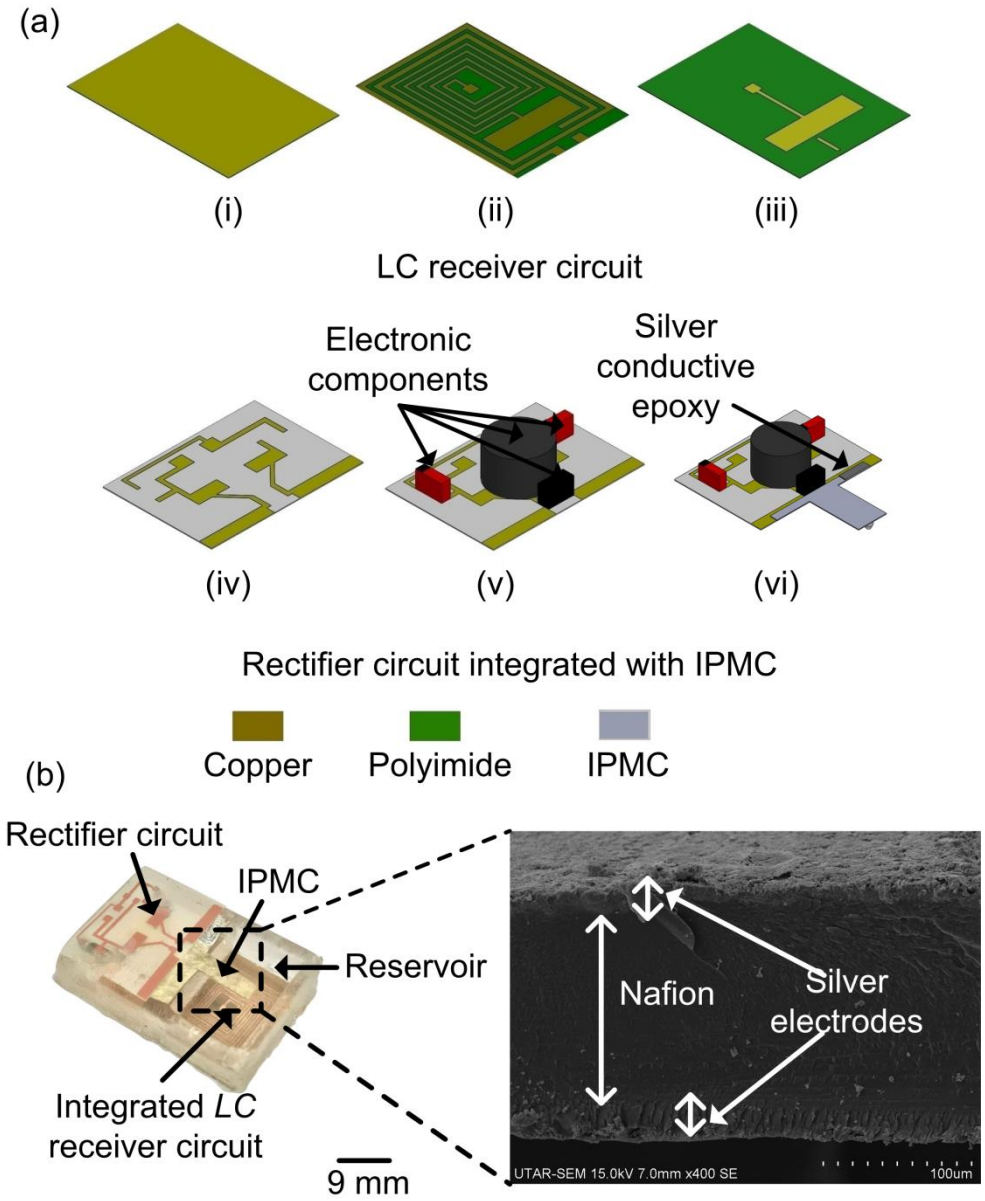

Figure 5.3: (a) Device fabrcation process (i) double layer Cu-clad sheet, (ii) forming of inductor and capacitor plate (top-view), (iii) forming of capacitor plate (bottom-view), (iv) etching of the rectifier circuit, (v) soldering of the electronic components and (vi) bonding the IPMC cantilever with rectifier circuit, and (b) Complete device and scanning electron microscopy (SEM) image of a cross-section of the IPMC layer

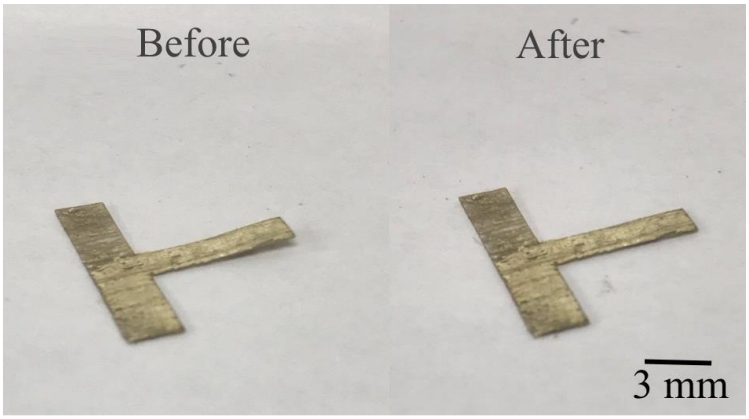

Figure 5.4: IPMC actuator before and after the low temperature annealing process

5.4 Experiment Results and Discussion

In this section, the wirelessly characterization results for the fabricated IPMC-based cantilever valve will be discussed. Wireless release test of the developed prototype was demonstrated using dye solution loaded in the device reservoir. In vitro study with human tumor cells (HeLa) were conducted to demonstrate the proof of concept of the developed potential implantable drug delivery device.

5.4.1 Experimental Setup

Demonstration of wirelessly controlled drug delivery was performed with the setup consisting of a square wave function generator (SFG-830, GW Instek, Taiwan) and a class-E power amplifier (output power of 0.65 W) that produced the magnetic field through the external transmitter connected to the amplifier. An oscilloscope (MDS1102CA, Matrix, China) was used to determine the electrical response of the LC receiver circuit. The setup also

involved a laser displacement sensor (CD5-85, Optex, Japan) and a load cell (FX300i, A&D, Japan) to characterize the displacement and force of the cantilever valve, respectively. As a preliminary experiment, the fabricated LC receiver circuit was examined for its frequency dependency, separation distance and tilting alignment with external transmitter. Wireless release test for visual demonstration were conducted by loading the device's reservoir with food dye solution. The device was immersed in a beaker filled with DI water and then placed on top of the external transmitter. The device was then activated by radiating an RF field from the external transmitter (Figure 5.5). Similar setup was utilized to measure the quantitative release of drug concentration from the developed device to an aqueous environment. This time, the device reservoir was filled with fluorescent solution (Sigma Aldrich, USA) and the liquid release was evaluated by a well-plate reader. In-*vitro* experiment was carried out by treating cervical tumor cells (HeLa Cells) with cisplatin to demonstrate the proof of concept of the developed device for drug delivery application. For the cell cultured experiment, both sterilized devices were loaded with Cisplatin and submerged in petri dishes filled with human cervix carcinoma cell line (HeLa) culture medium (mixture of 90% RPMI (Sigma Aldrich, USA) and 10% of fetal bovine serum (FBS) (Sigma Aldrich, USA). RF field was activated at one petri dish whereas another petri dish serves as a control sample (RF turned off). Both cell culture media were collected after 10 minutes of RF activation and transferred to 96 well-plates (Greiner 96 Flat Bottom Transparent Polystyrene, Sigma Aldrich, USA), which have HeLa cells cultured at a seeding density of 7000 cells/well. To examine the cell viability, 10% concentration of MTT assay (Sigma Aldrich,

USA) was added into the well with the volume 10 µL and incubated in a 5% CO2 incubator (HERAcell 150, Thermo (Heraeus), Germany) at 30 ℃ for 1, 3 and 24 hours. All experiments were carried out in the Biosafety cabinet (BIO II A, Telstar, Spain).

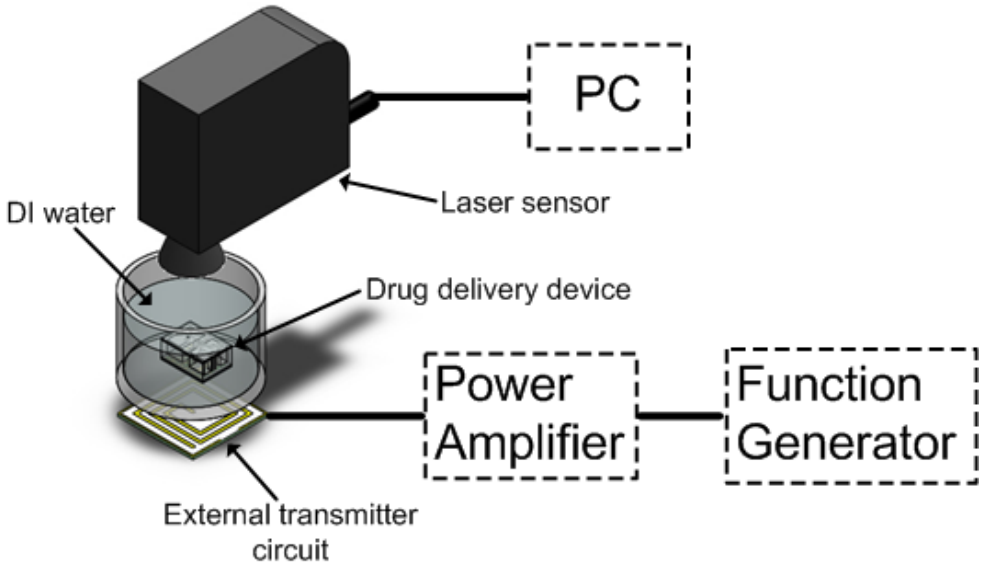

Figure 5.5: Experimental setup for wireless RF controlled drug delivery device. The data acquisition system involved the laser sensor which was used to detect the deformation of the IPMC cantilever and a computer for data acquisition

5.4.2 Wireless Test of the IPMC-based Cantilever Valve

IPMC-based cantilever consists of an ion exchange sheet clamped with two silver electrode plates, behaving as a capacitor in a lumped mass model (Abdelnour et al., 2012). An impedance analysis was conducted to identify the capacitive behaviors of the IPMC-based cantilever with a 10 Ω shunt resistor connected in series at multiple wireless DC step voltages of 1 V, 2 V and 3 V (maximum DC voltage from the DC rectifier circuit). The current induced at the IPMC-based

cantilever was experimentally measured using a data acquisition module (Elvis board II, National Instruments, U.S). The current increases rapidly at each step voltage changes and slowly decreases to its steady state, Figure 5.6(a). This can be explained from the lumped mass model, where the current (corresponding to the motion of cations in the IPMC-based cantilever) stop flowing when it reaches equilibrium. The charge stored in the IPMC cantilever are proportional to the produced deflection, and thus controlling the actuating behaviour of the IPMC cantilever.

Figure 5.6(b) shows that the IPMC cantilever tip displacement and block force increase with increasing applied voltage, measured by immersing the developed device in a beaker filled with DI water which was placed on top of the transmitter circuit. The measurement shows a deflection of approximately 11 um with the tip force of 0.1 mN at 1 Vdc induced voltage of the LC receiver circuit. Below 1 Vdc, the IPMC cantilever does not show any noticeable displacement as the low voltage is not able to initiate any cations' motion.

The tip force increases to 0.36 mN and 0.72 mN for 2 Vdc and 3 Vdc, respectively. Previous study has shown that the tip force can be enhanced by thickening the ion exchange membrane (Kim et al., 2007). The cost and complex manufacturing processes, nonetheless, are other issues to be taken into consideration. Figure 5.6(c) shows the response of the IPMC actuator activated in 3 sets of repeated RF ON-OFF cycles: 10

seconds RF ON, 10 seconds RF OFF with ~3 Vdc output voltages. A cantilever displacement of 66 μm was measured at the 10th second of RF ON activation. The cantilever deflection, however, experiences a slight increase to 70 μm at the end of the RF OFF cycle. This behavior repeats until the end of the experiment with the cumulative deflection values of 110 μm and 160 μm for the second and third cycle, respectively. To examine the increase of IPMC displacement phenomenon at each RF OFF cycle, the voltage profile at the IPMC actuator is shown in Figure 5.6(c). The voltage slightly decreases after the 3th second at the first RF ON cycle due to capacitive effect, Figure 5.6(a).

On the other hand, the voltage decreases abruptly at the RF OFF cycle to approximately 2 Vdc. Figure 5.6(d) shows the voltage time response of the rectifier circuit in one RF ON/OFF cycle, which verifies the capacitive properties in the DC rectifier circuit. Figure 5.6(b) shows that the IPMC actuator deflects at approximately 2 Vdc and therefore resulting in increasing cumulative IPMC actuator displacement in the RF OFF cycle. IPMC actuator remains at its final position if no voltage is applied across the membrane.

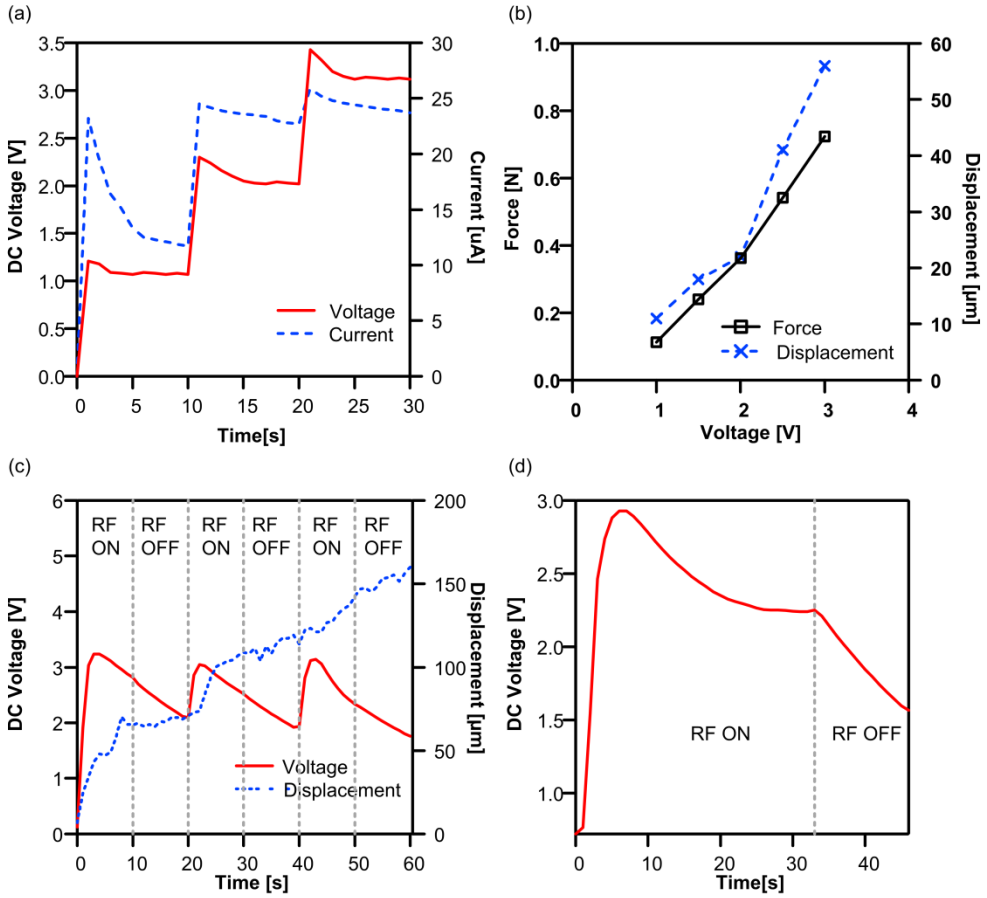

Figure 5.6: Wireless characterization of the IPMC cantilever valve (a) Current response of the IPMC actuator with step voltage of 1 Vdc, 2 Vdc 3 Vdc, (b) IPMC actuator block force and tip displacement response with step voltage of 1 V, 2 V, 3 V, (c) IPMC actuator tip displacement and DC voltage versus time with responded to 10 s RF ON / 10 s RF OFF activation, and (d) Voltage response of rectifier circuit activated in one RF ON/OFF cycle

5.4.3 Wireless Release Demonstration

As a preliminary test of wireless drug release for visual verification, a prototype with a reservoir filled with the dye solution was placed in a water-filled beaker and then activated with a RF field from an external transmitter circuit. Figure 5.5 shows the setup used for this experiment. In this setup, the device was activated for 2 minutes by tuning the field frequency that supplied to the transmitter circuit to 25 MHz with 20 V_{pp}. In Figure 5.7(a), the

prototype functions as a control sample to show no detachable release of dye from the device when the wireless power is turned off. The device is activated in Figure 5.7(b) and it can be visually observed that at the 17th second, a significant amount of dye release is initiated due to the pressure pushed by the IPMC cantilever. The dye is then sunk and condensed at the released hole of the device at the 20th seconds in DI water Figure 5.7(c). When time elapses, the released of dye continues and starts to diffuse to the environment. More dye release is observed in Figure 5.7(d) at time 1.55 min. This experiment verifies that the fabricated device operates properly with frequency tuning.

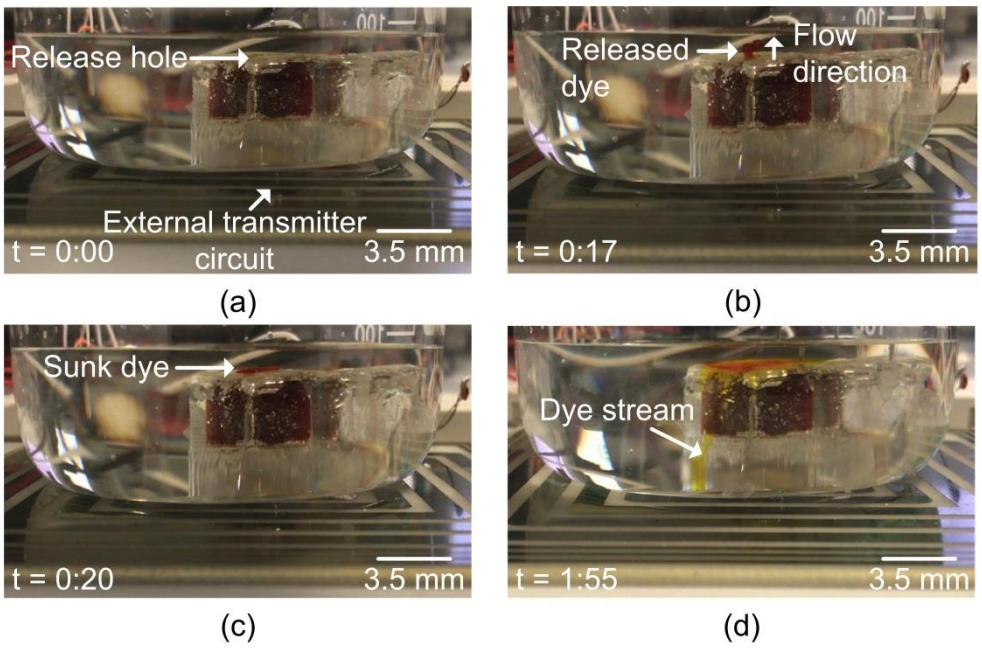

Figure 5.7: Preliminary wireless release test of the drug delivery device preloaded with color dye (a) t = 0:00, (b) t = 0:17, (c) t = 0:20, and (d) t = 1:55

5.4.4 In-Vitro Study

The quantitative release of drug concentration from the developed device to an aqueous environment was tested by measuring the fluorescent solution (Sigma Aldrich, USA) for every 10 s using a well-

plate reader. All the measurements were performed without agitation or forced flow. Prior to device activation, leak test was performed with the device fully filled with fluorescein and immersed in DI water without turning on the RF power. Figure 5.8(a) shows no distinct increase in intensity for the mentioned period, suggesting there is negligible off-state leakage of fluorescein to the environment. The intensity increases in a cumulative and incremental manner at RF ON with the power of 0.4 W and 0.6 W at an average released rate of ~0.06 μL/s and ~0.1 μL/s, respectively. The results clearly demonstrate that tuned RF activation of the device is effective in performing fluorescein released using the wireless approach.

To demonstrate the proof of concept of wirelessly activated drug delivery, *in-vitro* experiment was carried out by treating cervical tumor cells (HeLa Cells) with cisplatin. Cisplatin is a chemotherapeutic drug for the treatment of cervical cancer (Horky et al., 2001, Lee et al., 2015, Ordikhani et al., 2016). Figure 5.8(b) illustrates the cell viability assay of the tumor cells with drug released from the developed prototype immersed in Fetal Bovine Serum with RF turned on for 10 minutes. The released drug solution was collected 10 minutes after releasing the drug and transferred to 96-well plate. The results indicate that the viability of the HeLa cells decreases significantly 1 to 3 hours after the wirelessly triggered release, following by gradually reduction to ~30% cell viability at 24 hours. Our developed prototype does not show any drug release at RF OFF. This control study proves that the death of HeLa cell is not associated with any passive leakage or device material, but

indeed by wirelessly controlled drug release. Figure 5.8(c) and (d) present HeLa cells morphologies at RF turned off (control) and RF turned on for 24 hours incubation periods, respectively. Healthy tumor cells are observed to form a cohesive cluster with well-shaped and smooth surface for RF turned off. The tumor cells, on the other hand, appear to be rounded and shrunken with some death cells when the RF is turned on.

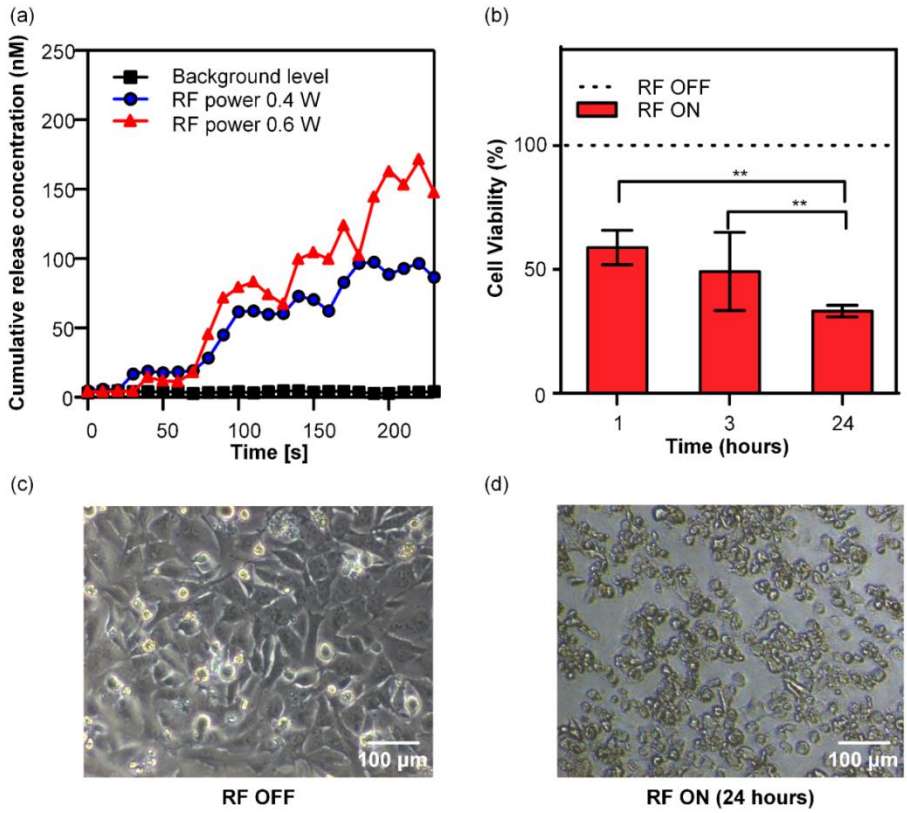

Figure 5.8: In vitro evaluations of the developed prototype in cell viability assay (MTT) using human tumor cells (HeLa) (a) Cumulative release of fluorescent concentration from the fabricated device at 0.4 W and 0.6 W, (b) Cell viability assay using Cisplatin drug released at RF turned off and on at different incubation times (Data is average + SD of 3 independent experiments. Asterisks denote statistical significant difference as compared to cell viability at 24 hours (Student's T test, **p<0.01), (c) Optical microscope images (scale bar: 100 um) of Hela cells at RF turned off, and (d) RF turned on (24 hours incubation time) configuration

5.5 Conclusion

The fully passive wireless activated IPMC-based cantilever valve soft drug delivery device is designed, fabricated and demonstrated with drug release operation triggered by an external RF magnetic field. The electroactive IPMC cantilever was integrated with a planar LC receiver circuit consisting of a resonator and load loops. The cantilever serves as the actuator to control the opening gap of the release orifice using input power from the transmitter. The wireless coupling effects of the encapsulated LC receiver circuit were examined and analysed, including resonant frequency study in multiple mediums and position orientation at the transmitter circuit. The IPMC cantilever deflection and force profile were characterized at different RF voltages and repeated RF ON-OFF cycles. A proof-of-concept release of Cisplatin drug from the fabricated prototype shows successful decrease of cell viability of HeLa cell with RF turned on. The future work will encompass the optimization of the device design and the further miniaturization of the device for lower loss and higher power transfer efficiency, as well as an in-vivo study in animals.

CHAPTER 6

CONCLUSION AND FUTURE WORKS

6.1 Conclusion

In this dissertation, a planar-based wireless RF magnetic field powered IPMC actuator has been proposed. To meet the research objectives for this project, the developed wireless powered IPMC has been applied to biomedical applications involved soft robotic microgripper and implantable drug delivery device. The experiment results validate the effectiveness of the developed prototypes toward the targeted applications.

In Chapter 3, the planar-based wireless RF magnetic field power transfer system was characterized in detail. The planar LC receiver circuit and DC rectifier circuit were constructed to miniaturize the size of the whole antenna. The resonant frequencies, S_{11} parameters of the LC receiver circuit in different mediums were experimentally analysed. The interaction behaviour between the transmitter and receiver circuits is also experimentally characterized.

In Chapter 4, the wireless powered IPMC using magnetic resonant coupling and its application to soft robotic microgripper was reported. The microgripper was designed to operate with one active finger (made of IPMC

actuator) and one stationary finger (made of Cu-clad PI sheet) to eliminate the misalign issues. The wireless response of the microgripper was experimentally characterized. The proof of concept of the developed microgripper in biological cell manipulation was performed wirelessly by gripping fish egg.

Chapter 5 has reported an implantable IPMC-based drug delivery device, which allows drug to be delivered at efficacious location to increase drug efficiency to combat targeted disease. The wirelessly activated IPMC-based cantilever valve was experimentally characterized. The device was loaded with dye solution and immersed in DI water to demonstrate the wireless drug release. Systematic in vitro study demonstrates the reduction of HeLa cell viability through the release of Cisplatin drug from the developed prototype. These results demonstrated the proof of concept of the wirelessly activated soft IPMC cantilever valve for mobile, reliable and safe targeted drug delivery.

6.2 Future Works

Based on the results reported in this dissertation, there are possible potential areas that can be further enhanced to optimise its performance. The size of the developed wireless system is an important factor to ensure portability. Hence, the LC receiver circuit can be further miniaturized using low temperature co-fired ceramic (LTCC) technology. Moreover, the power losses of the wireless power transfer system might degrade the devices' performance. Future work such as impedance matching is suggested to

increase the power transfer efficiency. The speed, force and displacement of the IPMC actuator are essential factors to ensure optimum performance in drug release and object gripping applications. For instance, insufficient of force generated by the IPMC actuator might cause failure of the drug release mechanism. The IPMC actuator can be optimized through simulation modelling to achieve high bending speed, large displacement and force.

PUBLICATION

Cheong, H.R., Lai, K.C. and Chee, P.S., 2018. A wireless powered electroactive polymer using magnetic resonant coupling. *IOP Conference Series: Materials Science and Engineering*, vol. 409, (1), p. 012002. (Best presentation award)

Cheong, H.R., Teo, C.Y., Leow, P.L., Lai, K.C. and Chee, P.S., 2018. Wireless-powered electroactive soft microgripper. *Smart Materials and Structures*, 27(5), p. 055014. (Impact factor: 2.963) (Q1)

Cheong, H.R., Nguyen, N-.T., Khaw, M.K., Teoh, B.Y., Chee, P.S., 2018. Wireless activated device with an integrated ionic polymer metal composite (IPMC) cantilever valve for targeted drug delivery. *Lab on a Chip*, 18(20), pp. 3207-3215. (Impact factor: 5.995) (Q1)

REFERENCE

Abdelnour, K., Stinchcombe, A., Porfiri, M., Zhang, J. and Childress, S., 2012. Wireless powering of ionic polymer metal composites toward hovering microswimmers. *IEEE/ASME Transactions on Mechatronics*, 17, (5), pp. 924-935.

Abid, A., O'Brien, J.M., Bensel, T., Cleveland, C., Booth, L., Smith, B.R., Langer, R. and Traverso, G., 2017. Wireless Power Transfer to Millimeter-Sized Gastrointestinal Electronics Validated in a Swine Model. *Scientific reports*, 7, p. 46745.

AFRIDI, K., 2018. Wireless Charging of Electric Vehicles. in *Frontiers of Engineering: Reports on Leading-Edge Engineering from the 2017 Symposium*.

Ali, M. and Sultan, M. 2012, 'Integration and wireless control methods for micromachined shape-memory-alloy actuators and their MEMS applications', University of British Columbia.

Ali, M.M. and Takahata, K., 2010. Frequency-controlled wireless shape-memory-alloy microactuators integrated using an electroplating bonding process. *Sensors and Actuators A: Physical*, 163, (1), pp. 363-372.

Arumugam, J. 2012, 'Ionic Polymer-Metal Composites: Thermodynamical Modeling and Finite Element Solution', Texas A & M University.

Baker, C.R., Armijo, K., Belka, S., Benhabib, M., Bhargava, V., Burkhart, N., Der Minassians, A., Dervisoglu, G., Gutnik, L. and Haick, M.B., 2007. Wireless sensor networks for home health care. in *Advanced Information Networking and Applications Workshops, 2007, AINAW'07. 21st International Conference on*, vol. 2, pp. 832-837.

Bar-Cohen, Y., Su, J., Harrison, J., Clair, T. and Leary, S., 1999. Electrostrictive Graft Elastomers and Applications.

Benmoussa, N., Guen, A., Bouazza, B. and Otmani, R., 2014. Electrostatic actuation of a silicon membrane to control the injected fluid volume by a micro pump. in *Dielectric Materials for Photovoltaic Systems (NAWDMPV), 2014 North African Workshop on*, pp. 1-4.

Bhandari, B., Lee, G.-Y. and Ahn, S.-H., 2012. A review on IPMC material as actuators and sensors: fabrications, characteristics and applications. *International journal of precision engineering and manufacturing*, 13, (1), pp. 141-163.

Bhattacharya, S., Bepari, B. and Bhaumik, S., 2016. Soft robotic finger fabrication with PDMS and IPMC actuator for gripping. in *SAI Computing Conference (SAI), 2016*, pp. 403-408.

Bhattacharya, S., Das, R., Chakraborty, R., Dutta, T., Mondal, A., Sarkar, S., Bepari, B. and Bhaumik, S., 2017. IPMC based data glove for object identification. in *Informatics, Electronics and Vision & 2017 7th International Symposium in Computational Medical and Health Technology (ICIEV-ISCMHT), 2017 6th International Conference on*, pp. 1-6.

Boys, J., Covic, G. and Green, A.W., 2000. Stability and control of inductively coupled power transfer systems. *IEE Proceedings-Electric Power Applications*, 147, (1), pp. 37-43.

Brown, W.C., 1984. The history of power transmission by radio waves. *IEEE Transactions on microwave theory and techniques*, 32, (9), pp. 1230-1242.

Cannon, B.L., Hoburg, J.F., Stancil, D.D. and Goldstein, S.C., 2009. Magnetic resonant coupling as a potential means for wireless power transfer to multiple small receivers. *IEEE transactions on power electronics*, 24, (7), pp. 1819-1825.

Carpi, F., Kornbluh, R., Sommer-Larsen, P., De Rossi, D. and Alici, G., 2011. Guest editorial introduction to the focused section on electroactive polymer mechatronics. *IEEE/ASME Transactions on Mechatronics*, 16, (1), pp. 1-8.

Chattaraj, R., Bhattacharya, S., Roy, A., Mazumdar, A., Bepari, B. and Bhaumik, S., 2014. Gesture based control of IPMC actuated gripper. in *Engineering and Computational Sciences (RAECS), 2014 Recent Advances in*, pp. 1-6.

Chatterjee, S., Fernando, W. and Wasantha, M., 2003. Adaptive modulation based MC-CDMA systems for 4G wireless consumer applications. *IEEE Transactions on Consumer Electronics*, 49, (4), pp. 995-1003.

Chee, P.S., Mah, C.K. and Ali, M.S.M., 2016. Soft dielectric elastomer actuator for micropump application. in *Micro Electro Mechanical Systems (MEMS), 2016 IEEE 29th International Conference on*, pp. 561-564.

Chen, Q., Xiong, K., Bian, K., Jin, N. and Wang, B., 2009. Preparation and performance of soft actuator based on IPMC with silver electrodes. *Frontiers of Mechanical Engineering in China*, 4, (4), pp. 436-440.

Chen, X., Assadsangabi, B., Hsiang, Y. and Takahata, K., 2018. Enabling Angioplasty‐Ready "Smart" Stents to Detect In‐Stent Restenosis and Occlusion. *Advanced Science*, 5, (5), p. 1700560.

Chen, Z., Shatara, S. and Tan, X., 2010. Modeling of biomimetic robotic fish propelled by an ionic polymer–metal composite caudal fin. *IEEE/ASME Transactions on Mechatronics*, 15, (3), pp. 448-459.

Cheng, Y.Z., Jin, J., Li, W.L., Chen, J.F., Wang, B. and Gong, R.Z., 2016. Indefinite-permeability metamaterial lens with finite size for miniaturized wireless power transfer system. *AEU-International Journal of Electronics and Communications*, 70, (9), pp. 1282-1287.

Cheong, H.R., Teo, C.Y., Leow, P.L., Lai, K.C. and Chee, P.S., 2018. Wireless-powered electroactive soft microgripper. *Smart Materials and Structures*, 27, (5), p. 055014.

De Gennes, P., Okumura, K., Shahinpoor, M. and Kim, K.J., 2000. Mechanoelectric effects in ionic gels. *EPL (Europhysics Letters)*, 50, (4), p. 513.

Deole, U., Lumia, R., Shahinpoor, M. and Bermudez, M., 2008. Design and test of IPMC artificial muscle microgripper. *Journal of Micro-Nano Mechatronics*, 4, (3), pp. 95-102.

Deyle, T. and Reynolds, M., 2008. Surface based wireless power transmission and bidirectional communication for autonomous robot swarms. in *Robotics and Automation, 2008. ICRA 2008. IEEE International Conference on*, pp. 1036-1041.

Fang, B.-K., Ju, M.-S. and Lin, C.-C.K., 2007. A new approach to develop ionic polymer–metal composites (IPMC) actuator: Fabrication and control for active catheter systems. *Sensors and Actuators A: Physical*, 137, (2), pp. 321-329.

Flack, F., James, E. and Schlapp, D., 1971. Mutual inductance of air-cored coils: Effect on design of radio-frequency coupled implants. *Medical and biological engineering*, 9, (2), pp. 79-85.

Ford, S., Macias, G. and Lumia, R., 2014. Single active finger IPMC microgripper. *Smart Materials and Structures*, 24, (2), p. 025015.

Fujita, H., 1989. Studies of micro actuators in Japan. in *Robotics and Automation, 1989. Proceedings., 1989 IEEE International Conference on*, pp. 1559-1564.

Geist, J., Shah, J.J., Rao, M.V. and Gaitan, M., 2007. Microwave power absorption in low-reflectance, complex, lossy transmission lines. *Journal of research of the National Institute of Standards and Technology*, 112, (4), p. 177.

Gensler, H., Sheybani, R., Li, P.-Y., Lo, R., Zhu, S., Yong, K.-T., Roy, I., Prasad, P.N., Masood, R. and Sinha, U.K., 2010. Implantable MEMS drug delivery device for cancer radiation reduction. in *Micro Electro Mechanical Systems (MEMS), 2010 IEEE 23rd International Conference on*, pp. 23-26.

Ghazali, F.A.M., Mah, C.K., AbuZaiter, A., Chee, P.S. and Ali, M.S.M., 2017. Soft dielectric elastomer actuator micropump. *Sensors and Actuators A: Physical*, 263, pp. 276-284.

Goldsmith, C., Ehmke, J., Malczewski, A., Pillans, B., Eshelman, S., Yao, Z., Brank, J. and Eberly, M., 2001. Lifetime characterization of capacitive RF MEMS switches. in *Microwave Symposium Digest, 2001 IEEE MTT-S International*, vol. 1, pp. 227-230.

Hines, L., Petersen, K. and Sitti, M., 2017. Asymmetric stable deformations in inflated dielectric elastomer actuators. in *Robotics and Automation (ICRA), 2017 IEEE International Conference on*, pp. 4326-4331.

Hoang, H. and Bien, F. 2012, *Maximizing efficiency of electromagnetic resonance wireless power transmission systems with adaptive circuits*, INTECH Open Access Publisher.

Horky, M., Wurzer, G., Kotala, V., Anton, M., Vojtesek, B., Vácha, J. and Wesierska-Gadek, J., 2001. Segregation of nucleolar components coincides with caspase-3 activation in cisplatin-treated HeLa cells. *Journal of Cell Science*, 114, (4), pp. 663-670.

Huber, J., Fleck, N. and Ashby, M., 1997. The selection of mechanical actuators based on performance indices. in *Proceedings of the Royal Society of London A: Mathematical, Physical and Engineering Sciences*, vol. 453, pp. 2185-2205.

Jain, R., Datta, S., Majumder, S. and Dutta, A., 2011. Two IPMC fingers based micro gripper for handling. *International Journal of Advanced Robotic Systems*, 8, (1), p. 13.

Jiaqi, W., McDaid, A., Lu, C. and Aw, K., 2016. A Compact Ionic Polymer-Metal Composite (IPMC) Actuated Valveless Pump for Drug Delivery. *IEEE/ASME Transactions on Mechatronics*.

Kim, B., Lee, M.G., Lee, Y.P., Kim, Y. and Lee, G., 2006. An earthworm-like micro robot using shape memory alloy actuator. *Sensors and Actuators A: Physical*, 125, (2), pp. 429-437.

Kim, H.J., Shin, J., Kang, S., Kim, S. and Tahk, M.-J., 2007. Ionic electroactive polymer control using co-evolutionary optimisation. *Electronics Letters*, 43, (16), pp. 859-860.

Kim, S.-H., Lim, Y.-S. and Lee, S.-J., 2013. Magnetic resonant coupling based wireless power transfer system with in-band communication. *JSTS: Journal of Semiconductor Technology and Science*, 13, (6), pp. 562-568.

Kkelis, G., Yates, D.C. and Mitcheson, P.D., 2015. Comparison of current driven Class-D and Class-E half-wave rectifiers for 6.78 MHz high power IPT applications. in *Wireless Power Transfer Conference (WPTC), 2015 IEEE*, pp. 1-4.

Ko, S.C., Kim, Y.C., Lee, S.S., Choi, S.H. and Kim, S.R., 2002. Piezoelectric membrane acoustic devices. in *Micro Electro Mechanical Systems, 2002. The Fifteenth IEEE International Conference on*, pp. 296-299.

Kurs, A., Karalis, A., Moffatt, R., Joannopoulos, J.D., Fisher, P. and Soljačić, M., 2007. Wireless power transfer via strongly coupled magnetic resonances. *science*, 317, (5834), pp. 83-86.

Lee, C.H., Kim, H., Harburg, D.V., Park, G., Ma, Y., Pan, T., Kim, J.S., Lee, N.Y., Kim, B.H. and Jang, K.-I., 2015. Biological lipid membranes for on-demand, wireless drug delivery from thin, bioresorbable electronic implants. *NPG Asia materials*, 7, (11), p. e227.

Lee, J.-W. and Yoo, Y.-T., 2011. Preparation and performance of IPMC actuators with electrospun Nafion®–MWNT composite electrodes. *Sensors and Actuators B: Chemical*, 159, (1), pp. 103-111.

Lee, S., Park, H., Pandita, S.D. and Yoo, Y., 2006. Performance improvement of IPMC (ionic polymer metal composites) for a flapping actuator. *International Journal of Control Automation and Systems*, 4, (6), p. 748.

Lei, H. and Tan, X., 2013. Fabrication and characterization of a two-dimensional IPMC sensor. in *Electroactive Polymer Actuators and Devices (EAPAD) 2013*, vol. 8687, p. 868707.

Li, X., Tsui, C.-Y. and Ki, W.-H., 2015. A 13.56 MHz wireless power transfer system with reconfigurable resonant regulating rectifier and wireless power control for implantable medical devices. *IEEE Journal of solid-state circuits*, 50, (4), pp. 978-989.

Lin, H.-H., Fang, B.-K., Ju, M.-S. and Lin, C.-C.K., 2009. Control of ionic polymer-metal composites for active catheter systems via linear parameter-varying approach. *Journal of Intelligent Material Systems and Structures*, 20, (3), pp. 273-282.

Lumia, R. and Shahinpoor, M., 2008. IPMC microgripper research and development. in *Journal of Physics: Conference Series*, vol. 127, p. 012002.

Mai, M., Ke, S., Lin, P. and Zeng, X., 2015. Ferroelectric polymer thin films for organic electronics. *Journal of Nanomaterials*, 16, (1), p. 181.

McDaid, A., Xie, S. and Aw, K., 2012. A compliant surgical robotic instrument with integrated IPMC sensing and actuation. *International Journal of Smart and Nano Materials*, 3, (3), pp. 188-203.

Merrill, R., Lee, T., You, H., Rasmussen, R. and Moberly, L., 1995. Optimization of high Q integrated inductors for multi-level metal CMOS. in *Electron Devices Meeting, 1995. IEDM'95., International*, pp. 983-986.

Mirfakhrai, T., Madden, J.D. and Baughman, R.H., 2007. Polymer artificial muscles. *Materials today*, 10, (4), pp. 30-38.

Moghadam, M.R.V. and Zhang, R., 2016. Multiuser wireless power transfer via magnetic resonant coupling: performance analysis, charging control, and power region characterization. *IEEE Transactions on Signal and Information Processing over Networks*, 2, (1), pp. 72-83.

Mohan, S.S., del Mar Hershenson, M., Boyd, S.P. and Lee, T.H., 1999. Simple accurate expressions for planar spiral inductances. *IEEE Journal of solid-state circuits*, 34, (10), pp. 1419-1424.

Mousavi, M.S.S., Karami, A.H., Kolahdouz, M., Manteghi, F. and Ataei, F., 2018. Design of a remote-control drug delivery implantable chip for cancer local on demand therapy using ionic polymer metal composite actuator. *Journal of the mechanical behavior of biomedical materials*.

Mukundan, V. and Pruitt, B.L., 2009. MEMS electrostatic actuation in conducting biological media. *Journal of Microelectromechanical Systems*, 18, (2), pp. 405-413.

Nelson, S.E., 2015. Feasibility Study of Custom Manufacturing of Ionic Polymer-Metal Composite Sensors.

Nguyen, K.T., Ko, S.Y., Park, J.-O. and Park, S., 2015. Terrestrial walking robot with 2DoF ionic polymer–metal composite (IPMC) legs. *IEEE/ASME Transactions on Mechatronics*, 20, (6), pp. 2962-2972.

Ong, Y.Y. 2016, 'Muscle-Alike Actuator based on Ionic Polymer Metal Composite (IPMC)', UTAR.

Ongaro, F., Yoon, C., van den Brink, F., Abayazid, M., Oh, S.H., Gracias, D.H. and Misra, S., 2016. Control of untethered soft grippers for pick-and-place tasks. in *Biomedical Robotics and Biomechatronics (BioRob), 2016 6th IEEE International Conference on*, pp. 299-304.

Ordikhani, F., Erdem Arslan, M., Marcelo, R., Sahin, I., Grigsby, P., Schwarz, J.K. and Azab, A.K., 2016. Drug delivery approaches for the treatment of cervical cancer. *Pharmaceutics*, 8, (3), p. 23.

Palmre, V., Pugal, D., Kim, K.J. and Yim, W., 2013. An electroactive IPMC-based cylindrical robotic platform. in *Ubiquitous Robots and Ambient Intelligence (URAI), 2013 10th International Conference on*, pp. 713-714.

Patrick, D.R. and Fardo, S.W. 2008, *Electricity and electronics fundamentals*, The Fairmont Press, Inc.

Pillarisetti, A., Anjum, W., Desai, J.P., Friedman, G. and Brooks, A.D., 2005. Force feedback interface for cell injection. in *Eurohaptics Conference, 2005 and Symposium on Haptic Interfaces for Virtual Environment and Teleoperator Systems, 2005. World Haptics 2005. First Joint*, pp. 391-400.

Pirmoradi, F.N., Jackson, J.K., Burt, H.M. and Chiao, M., 2011. On-demand controlled release of docetaxel from a battery-less MEMS drug delivery device. *Lab on a Chip*, 11, (16), pp. 2744-2752.

Ru, J., Zhu, Z., Wang, Y., Chen, H. and Li, D., 2018. Tunable actuation behavior of ionic polymer metal composite utilizing carboxylated carbon nanotube-doped Nafion matrix. *RSC Advances*, 8, (6), pp. 3090-3094.

Sarraf, E., Wong, G. and Takahata, K., 2009. Frequency-selectable wireless actuation of hydrogel using micromachined resonant heaters toward implantable drug delivery applications. in *Solid-State Sensors, Actuators and Microsystems Conference, 2009. TRANSDUCERS 2009. International*, pp. 1525-1528.

Shaari, M.F., Saw, S. and Samad, Z., 2014. Fabrication and characterization of lPMC actuator for underwater micro robot propulsor. *Applied Mechanics and Materials*, 575, pp. 716-720.

Shahinpoor, M. 2015, *Ionic Polymer Metal Composites (IPMCs): Smart Multi-Functional Materials and Artificial Muscles*, vol. 2, Royal Society of Chemistry.

Shahinpoor, M. and Kim, K.J., 2001. Ionic polymer-metal composites: I. Fundamentals. *Smart Materials and Structures*, 10, (4), p. 819.

Shahinpoor, M. and Kim, K.J., 2004. Ionic polymer–metal composites: III. Modeling and simulation as biomimetic sensors, actuators, transducers, and artificial muscles. *Smart Materials and Structures*, 13, (6), p. 1362.

Shen, L., Cha, Y., Shams, A. and Porfiri, M., 2013. Fabrication and buckling analysis of ionic polymer metal composite pipes. *Smart Materials and Structures*, 22, (10), p. 105032.

Si, P., Hu, A.P., Malpas, S. and Budgett, D., 2008. A frequency control method for regulating wireless power to implantable devices. *IEEE transactions on biomedical circuits and systems*, 2, (1), pp. 22-29.

Sridhar, V. 2008, 'A micromachined inductive sensor using folded flex-circuit structures and its wireless telemetry applications', University of British Columbia.

Stalbaum, T., Nelson, S.E., Palmre, V. and Kim, K.J., 2014. Multi degree of freedom IPMC sensor. in *Electroactive Polymer Actuators and Devices (EAPAD) 2014*, vol. 9056, p. 90562J.

Suma, N., Nagaraja, V.S., Pinjare, S., Neethu, K. and Sudharshan, K., 2012. Design and characterization of MEMS thermal actuator. in *Devices, Circuits and Systems (ICDCS), 2012 International Conference on*, pp. 638-642.

Valtchev, S.S., Baikova, E.N. and Jorge, L.R., 2012. Electromagnetic field as the wireless transporter of energy. *Facta universitatis-series: Electronics and Energetics*, 25, (3), pp. 171-181.

Vinge, R., 2015. Wireless Energy Transfer By Resonant Inductive Coupling. *Master of science thesis. Sweden, Goteborg*, p. 83.

Wakimoto, S., Suzumori, K. and Ogura, K., 2011. Miniature pneumatic curling rubber actuator generating bidirectional motion with one air-supply tube. *Advanced Robotics*, 25, (9-10), pp. 1311-1330.

Wang, Y., Chen, H., Wang, Y., Liu, J. and Li, D., 2013. Manufacturing process for patterned IPMC actuator with millimeter thickness. in *Assembly and Manufacturing (ISAM), 2013 IEEE International Symposium on*, pp. 235-239.

Xu, D., Wang, L., Ding, G., Zhou, Y., Yu, A. and Cai, B., 2001. Characteristics and fabrication of NiTi/Si diaphragm micropump. *Sensors and Actuators A: Physical*, 93, (1), pp. 87-92.

Yue, C.P., Ryu, C., Lau, J., Lee, T.H. and Wong, S.S., 1996. A physical model for planar spiral inductors on silicon. in *Electron Devices Meeting, 1996. IEDM'96., International*, pp. 155-158.

Zainal, M., Ahmad, A. and Ali, M.M., 2017. Frequency-controlled wireless shape memory polymer microactuator for drug delivery application. *Biomedical microdevices*, 19, (1), p. 8.

Zainal, M. and Ali, M.M., 2016. Wireless shape memory polymer microactuator for implantable drug delivery aplication. in *Biomedical Engineering and Sciences (IECBES), 2016 IEEE EMBS Conference on*, pp. 76-79.

Zamyad, H., Naghavi, N. and Barmaki, H., 2018. A combined fuzzy logic and artificial neural network approach for non‐linear identification of IPMC actuators with hysteresis modification. *Expert Systems*, p. e12283.

Zhang, L., Yang, Y. and Soh, C. 2012, 'IPMC-Based Biomedical Applications', in *Smart Materials in Structural Health Monitoring, Control and Biomechanics*, Springer, pp. 533-567.

Zhang, Y., Ma, C. and Dai, L., 2007. Electrode preparation and electro-deformation of ionic polymer-metal composite (IPMC). in *Nano/Micro Engineered and Molecular Systems, 2007. NEMS'07. 2nd IEEE International Conference on*, pp. 68-71.